Department of Electronics and Nanoengineering

Affordable light-trapping metamaterials for thin-film photovoltaic cells

Mikhail Omelyanovich

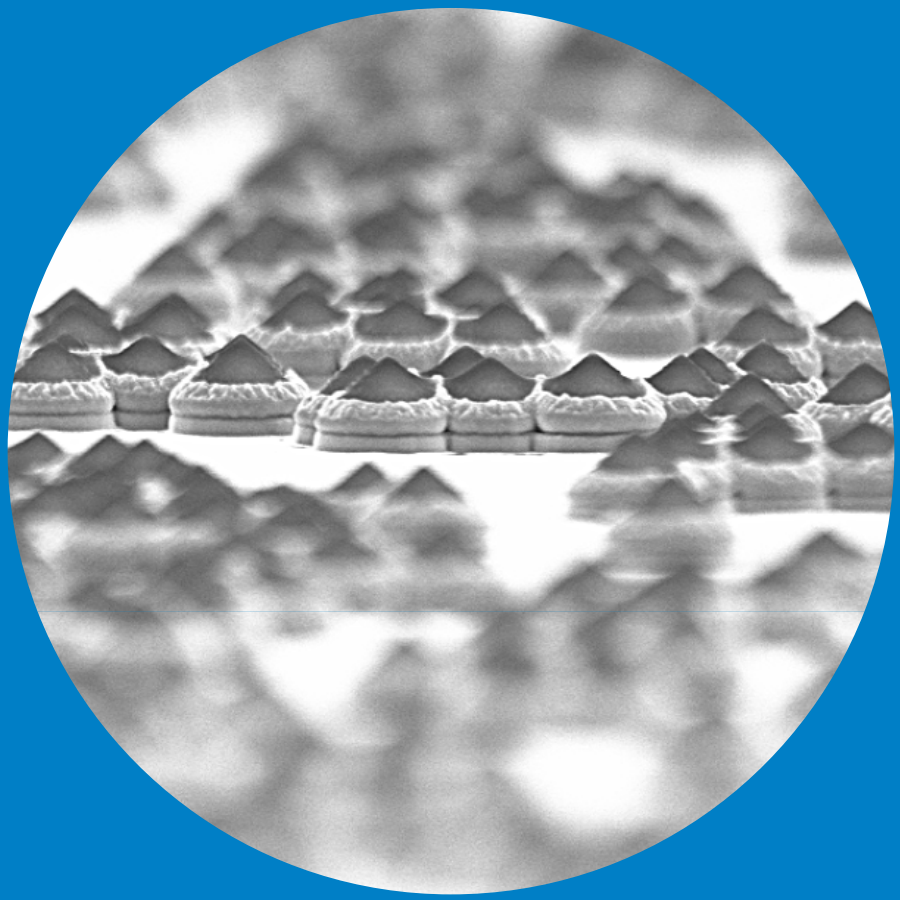

Aalto University

DOCTORAL DISSERTATIONS

Aalto University publication series
DOCTORAL DISSERTATIONS 37/2018

Affordable light-trapping metamaterials for thin-film photovoltaic cells

Mikhail Omelyanovich

A doctoral dissertation completed for the degree of Doctor of Science (Technology) to be defended, with the permission of the Aalto University School of Electrical Engineering, at a public examination held at the lecture hall TU2(Maarintie 8) of the school on 16 March 2018 at 12.

Aalto University
School of Electrical Engineering
Department of Electronics and Nanoengineering

Supervising professor
Prof. Constantin Simovski, Aalto University, Finland

Preliminary examiners
Prof. Aldo Di Carlo, University of Rome "Tor Vergata", Italy
Dr. Teemu Hakkarainen, Tampere University of Technology, Finland

Opponent
Prof. Andrei Lavrinenko, Technical University of Denmark, Denmark

Aalto University publication series
DOCTORAL DISSERTATIONS 37/2018

ISBN 978-952-60-7869-4 (printed)
ISBN 978-952-60-7870-0 (pdf)
ISSN-L 1799-4934
ISSN 1799-4934 (printed)
ISSN 1799-4942 (pdf)
http://urn.fi/URN:ISBN:978-952-60-7870-0

Images: 18

Unigrafia Oy
Helsinki 2018

Finland

441 697
Printed matter

Aalto University

Abstract

Aalto University, P.O. Box 11000, FI-00076 Aalto www.aalto.fi

Author
Mikhail Omelyanovich

Name of the doctoral dissertation
Affordable light-trapping metamaterials for thin-film photovoltaic cells

Publisher School of Electrical Engineering

Unit Department of Electronics and Nanoengineering

Series Aalto University publication series DOCTORAL DISSERTATIONS 37/2018

Field of research Radio Engineering

Manuscript submitted 6 November 2017 **Date of the defence** 16 March 2018

Permission to publish granted (date) 15 February 2018 **Language** English

☐ **Monograph** ☒ **Article dissertation** ☐ **Essay dissertation**

Abstract

The thesis reports on my doctoral studies in the field of light-trapping structure for planar multilayer thin-film photovoltaic diodes. In this report we consequently pass from plasmonic light-trapping structures enhancing the PV absorption of photodiodes in a narrow band to broadband all-dielectric light-trapping structures which were fabricated and successfully tested experimentally.

The first part of the thesis is focused on a novel regime of perfect absorption in a thin plasmonic layer that corresponds to a collective mode of a plasmonic nanosperes array. In the theoretical study we show that the absorption of the incident light occurs mainly in the semiconductor material hosting plasmonic nanospheres, whereas the absorption in the metal is negligible. The regime remains the same when the uniform host layer is replaced by a practical photovoltaic cell. Trapping the light allows the thickness of the doped semiconductor to be reduced to such values that the degradation under light exposure becomes insufficient. The light-trapping regime is compatible with both variants: the metal-backed photovoltaic cell and its semitransparent counterpart when both electrodes are made of a conductive oxide. Negligible parasitic losses, a variety of design solutions and a reasonable operational band make our perfect plasmonic absorbers promising for photovoltaic applications.

The second part of the thesis is devoted to synthetic perovskites with photovoltaic properties that opens a new era in solar photovoltaics. Due to high optical absorption perovskite-based thin-film solar cells are usually considered as absorbing solar radiation fully under conditions of ideal blooming. However, actually this assumption does not hold. In this part of the thesis we show that it is possible to cure this shortage by complementing the basic structure with an inexpensive plasmonic array of nanospheres.

The last research problem studied in the thesis is the dielectric metamaterial as an efficient light-trapping structure. It is shown theoretically that this metamaterial can decrease the reflection and simultaneously suppress the transmission through the photovoltaic layer because it transforms the incident plane wave into a set of focused light beams. This theoretical concept has been strongly developed and experimentally confirmed in the experimental work. Also the experiments show that a submicron layer of a transparent conducting oxide may act as a top electrode of a photovoltaic cell based on amorphous silicon when properly patterned by notches becomes an efficient light-trapping structure. The nanopatterning is achievable in a rather easy and affordable way that makes developed method of the solar cell enhancement attractive for industrial adaptation.

Keywords light-trapping, metamaterials, solar cells, microfabrication

ISBN (printed) 978-952-60-7869-4 **ISBN (pdf)** 978-952-60-7870-0

ISSN-L 1799-4934 **ISSN (printed)** 1799-4934 **ISSN (pdf)** 1799-4942

Location of publisher Helsinki **Location of printing** Helsinki **Year** 2018

Pages 128 **urn** http://urn.fi/URN:ISBN:978-952-60-7870-0

Preface

The research presented in this thesis has been carried out at the Department of Electronics and Nanoengineering of Aalto University, School of Electrical Engineering.

My warmest gratitude goes to my supervisor, Prof. Constantin Simovski, for his guidance and persistent help. He gave me a chance to work on this interesting topic and shared his ideas referring to this field with me.

Secondly, I would like to thank Prof. Pavel Belov. Without his help I would not succeed with my doctoral studies. He has attentively followed my progress and some measurements of my structures that could not be performed in Aalto University were done in St. Petersburg, in his Department of Nanophotonics referring to ITMO University.

Last but not the least I would like to thank my practical micro- and nanofabrication teacher Dr. Viktor Ovchinnikov. Thanks for fruitful discussions and sharing your experience in the field.

I am grateful to the present and former members of our research group: Prof. Sergei Tretyakov, Dr. Igor Nefedov, Dr. Mohammad Albooyeh, Dr. Younes Radi, Dr. Mohammad Sajjad Mirmoosa, Dr. Viktar Asadchy, Dr. Joni Vehmas, Mr. Pavel Voroshilov, Dr. Sergey Kosulnikov, Dr. Ana Diaz-Rubio, Dr. Fu Liu, Mrs. Svetlana Tcvetkova, Mr. Xuchen Wang and their relatives. We all were like one big family here and these four years were an excellent time in my life. Thank you all for your help and interesting discussions especially during our daily tea/coffee breaks.

I would like to express my gratitude to all my friends who are here and far away.

Special thanks go to my mother Tatiana, because only her hard work and her pushing me made this manuscript come true.

I address my warmest gratitude to my parents-in-law Anatoliy and Natalia, for supporting my lovely wife during all my business trips.

Finally, I wish to express my sincere thanks to my dear wife Daria for being with me and for the joy of raising our kid Lukas. Notice, that I met Daria here, in Finland, when I was moving towards this thesis.

Espoo, February 20, 2018,

Mikhail Omelyanovich

Contents

Preface **2**

Contents **4**

List of Publications **7**

Author's Contribution **8**

List of Abbreviations **10**

List of Symbols **11**

1. Introduction and literature survey **12**

1.1 Solar cells 12

1.1.1 Solar photovoltaic industry 12

1.1.2 Modern challenges of thin-film solar photovoltaic industry 14

1.1.3 About PV diodes 16

1.1.4 Solar cells as ultra-broadband PV diodes 18

1.1.5 Optical efficiency of thin-film solar cells 20

1.1.6 Advantages and disadvantages of thin-film solar cells 24

1.1.7 Excitonic PV devices and perovskite solar cells 25

1.2 Light-trapping for thin-film solar cells 26

1.2.1 Resonant light-trapping structures 28

1.2.2 What is my thesis about 30

1.3 Micro- and nanotechnologies in the fabrication of light-trapping structures 31

2. Plasmonic Metamaterial for Enhancement of a-Si Photodiodes **33**

2.1 Metal nanoparticles for absorption outside the metal 33

2.1.1 Biomedical application of a-Si photodiodes 33
2.1.2 Plasmonic perfect absorber operating as Huygens' metasurface 34
2.2 Local field concentration and enhancement of useful absorption 37
2.3 About practical implementation of the metamaterial photodiode 43

3. Affordable Plasmonic LTSs for Perovskite Solar Cells. 44
3.0.1 Perovskite as a photovoltaic absorber 44
3.1 Perovskite thin-film solar cells enhanced by metallic particles 46

4. Ultra-broadband wide-angle light-trapping by micron-sized spheres. 51
4.1 Colloidal nanoparticles for enhancement of thin-film solar cells based on amorphous silicon 51
4.1.1 Technical solution and its physical prerequisites . . . 51
4.2 Theoretical analysis of enhancement granted by our metamaterial: comparison with anti-reflecting coating 54
4.3 Experiment 57
4.3.1 Discussion of the cell geometry 57
4.3.2 Fabrication 58
4.3.3 Measurements 59
4.4 Conclusions for ultra-broadband wide-angle light-trapping by micron-sized spheres. 62

5. Ultra-broadband wide angle light-trapping structures implemented in the top electode 63
5.1 From spheres to hemispheres 63
5.2 Experimental and further numerical studies 66
5.2.1 Fabrication method and the obtained structure 68
5.2.2 Post-fabrication simulations and discussion 69
5.2.3 Measurement results and conclusions 70

6. Summary of Publications 73

7. Conclusions 75

References 77

Errata 85

Publications **87**

List of Publications

This thesis consists of an overview and of the following publications which are referred to in the text by their Roman numerals.

I Mikhail Omelyanovich, Younes Ra'di and Constantin Simovski, "Perfect plasmonic absorbers for photovoltaic applications," *Journal of Optics*, no. 17, p. 125901, October 2015.

II Mikhail Omelyanovich, Makarov, S., Milichko, V. and Constantin Simovski, "Enhancement of Perovskite Solar Cells by Plasmonic Nanoparticles," *Materials Sciences and Applications*, vol. 7, pp. 836–847, December 2016.

III Mikhail Omelyanovich, Viktor Ovchinnikov and Constantin Simovski, "A non-resonant dielectric metamaterial for the enhancement of thin-film solar cells," *Journal of Optics*, no. 17, p. 025102, January 2015.

IV Mikhail Omelyanovich and Constantin Simovski, "All Angle Light-Trapping Electrode for Photovoltaic Cells," *Optics Letters*, vol. 42, no. 20, p. 3726-3729, September 2017.

Author's Contribution

Publication I: "Perfect plasmonic absorbers for photovoltaic applications"

The author and Younes. Ra'di did the analytical and numerical calculations, and prepared the content for the manuscript. Professor Simovski supervised the work and assisted in the paper writing.

Publication II: "Enhancement of Perovskite Solar Cells by Plasmonic Nanoparticles"

The author had the leading role in development of the idea, and calculations. Mr. Makarov and Mr. Milichko helped the author in practical focus of the device, and Prof. Simovski supervised the work and assisted in the paper writing.

Publication III: "A non-resonant dielectric metamaterial for the enhancement of thin-film solar cells"

The author did the analytical and numerical calculations, and prepared the content for the manuscript. Dr. Ovchinnikov helped the author in practical realisation the structure, and Prof. Simovski supervised the work and assisted in the paper writing.

Publication IV: "All Angle Light-Trapping Electrode for Photovoltaic Cells"

The author was the responsible person for developing the idea and prepar-

ing the content for the manuscript. Prof. Simovski supervised the work and assisted in the paper writing.

List of Abbreviations

A	Ampere
AZO	Aluminium-doped zinc oxide
ALD	Atomic layer deposition
C	Celsius
cm	Centimetre
eV	Electronvolt
IBE	Ion beam etching
IR	Infrared
ITO	Indium tin oxide
MM	Metamaterial
m	Metre
nm	Nanometre
OL	Optical Lithography
PV	Photovoltaic
PVD	Physical Vapor Deposition
PECVD	Plasma-enhanced chemical vapour deposition
RIE	Reactive Ion Etching
s	Second
SC	Solar cell
TCO	Transparent conductive oxide
TE	Transverse electric
TM	Transverse magnetic
TFSC	Thin-film solar cells
W	Watt

List of Symbols

a	Absorption coefficient
c	Speed of light
$\mathbf{E}$	Electric field
E_{g}	Bandgap energy
e	Electric charge
f_{v}	Volume fraction
$\hbar$	Planck's constant
I	Current
$IQE(\omega)$	Internal Quantum Efficiency
k_0	Free-space wave number
k_{B}	Boltzmann constant
$\mathcal{P}_{\mathrm{elec}}$	Output electric power
$SR(\omega)$	Spectral response
V	Voltage
ε	Relative permittivity of a medium
ε_0	Free-space permittivity
η	Photovoltaic conversion efficiency
η_{UE}	Ultimate efficiency of a solar cell
λ	Wavelength
ω	Angular frequency
ω_{g}	Bandgap angular frequency

1. Introduction and literature survey

1.1 Solar cells

Light energy may be converted into electricity in various ways. In this thesis we concentrate on commonly-known photovoltaic (PV) conversion of light to electric current, also called photoelectric conversion. This conversion is based on the PE effect discovered in XIX century by A.Einstein. Further, technologies of purifying the semiconductors elaborated in 1950s allowed to obtain high-quality semiconductors really suitable for generation of electricity under the illumination by sunlight. These novel materials gave birth to solar photovoltaics – generation of electricity involving the PV effect [1]. Most part of solar cells (SCs) are photodiodes, though other devices performing the PV conversion of light are also known (see below). Photodiodes are used not only for generation of electric power – the effect can be used for sensing purposes [2], for optical control of automata [3] and for signal processing in optoelectronics [4]. The main peculiarity of SCs compared to other PV diodes is that the PV conversion covers a significant part of the solar frequency spectrum that is ultra-broad [1]. Therefore, SCs comprise passive components enhancing their optical efficiency in this ultra-broad band. Another peculiarity is arraying the PV diodes connected so that to transfer the maximal power to the external load. These big modules of SCs are called solar panels.

1.1.1 Solar photovoltaic industry

The development of solar photovoltaics since 1950s has been accompanied by enhancement of the overall efficiency of SCs, and resolving the key technological and management issues, such as: cost reduction, extension of the solar panel service life, improvement of its operation stability

in terrestrial outdoor applications, including domestic sources of electricity and solar electric stations, and in space applications with their specific ambient. Historically, the first commercialized solar cells had the overall efficiency close to 6% and were crystalline silicon (c-Si) solar panels with SCs protected of the hailstones and rain by glass plates [1]. Nowadays SCs based o c-Si and their Ge-based and GaAs-based counterparts are still produced (where glass plates are replaced by polymer laminate and novel technical solutions are used for reduction of internal and optic losses). Such SCs type where the PV conversion holds in a bulk monocrystal semiconductor are all photodiodes and referred as first-generation SCs. Silicon solar cells dominate in the solar PV market occupying 90% of it. They exhibit, on the average, overall efficiency of about 20% that has grown from 19.5% in 2004 [5] to 22.1% in 2014 [8]. It is clear that the fight for percents in the efficiency of these basic SCs is close to saturation. Nowadays there is a strong demand of a qualitative improvement in solar photovoltaics because SCs of the first generation have several drawbacks: still rather high fabrication cost, heavy weight reducing the demand for domestic needs, and hard implementation making the conformal placement of these SCs on curved surfaces impossible. Finally, there is toxicity in production and an amount of toxic waste, accompanying the fabrication of SCs. At least, it is so for SCs based on GaAs and Ge (10 years ago it was also so for Si SCs).

Attempts to eliminate these disadvantages led to the development of alternative SCs, including thin-film solar cells (TFSCs) which are now referred to as second-generation cells [1, 5]. These SCs are usually made of amorphous silicon (a-Si) that is the cheapest PV material and its production does not result in toxic waste. There are also TFSCs based on microcrystalline silicon (mc-Si) and on polycrystalline Si. Tandems of mc-Si and a-Si unlike other tandem SCs do not demand expensive monolithic technologies and are cheaper than SCs based on c-Si. These tandems are called micromorph SCs [5, 6]. Also one developed TFSCs based on compound semiconductors of III-V type (GaP, InP, GaAs) and II-VI type (CdTe). Nearly 15 years ago one started to fabricate TFSCs based on such compound semiconductors as copper indium selenide (CIS), copper indium gallium selenide (CIGS), and CuZnSnS (CZTS) [4, 5].

Several disadvantages inherent in the first-generation SCs were eliminated in TFSCs. Their fabrication requires less raw materials and consumes less energy, and they are easier to produce in large area than crys-

tal SCs. It is especially so, if the solar panel is flexible e.g. the mechanical carrier is metal foil or a plastic films. Such solar panel not only can be accommodated conformal on a non-planar surfaces, it can be also produced with the use of roll-to-roll technology very promising for mass production [7]. These merits led to the rapid development of second-generation SCs utilizing especially TFSCs based on a-Si [5] because they are cheapest ones and can be easily implemented on a flexible substrate.

Meanwhile, the overall efficiency of TFSCs industrially adapted 5-10 years ago was on the rather low level – from 4-5% for flexible TFSCs based on a-Si to 10-12% for best TFSCs implemented on a hard substrate – micromorph TFSCs and SCs based on compound semiconductors (CdTe, GaP, etc.) [8].

1.1.2 Modern challenges of thin-film solar photovoltaic industry

Nowadays in the photovoltaic industry you can follow several emerging technologies such as: multi-junction concentrator solar cells, the multi-junction SCs and black silicon SCs. The first one holds the current world record for SC efficiency(46%), the second one dominates in the space PV market where the power/weight ratio is more important compared to power/price. The third one addresses both issues allowing a significant decrease of the reflection loss for the case when the solar panel does not rotates after Sun and is impinged mainly by the obliquely incident light. As to thin-film solar photovoltaics, it experiences a decline.

Four years ago, when my doctoral studies started in Aalto University, TFSCs were on the peak of their development and presented a point of keen interest for industry and research institutes. Of course, the commercialized crystalline silicon solar photovoltaics with its daytime-averaged 20% efficiency is 2-4 times more efficient than the thin-film solar photovoltaics is. However, it is also more expensive, heavy and not conformal. Five years ago the difference in prices per unit area of a crystalline silicon solar cell and of a micromorph or CdTe solar cell was as high as 10 times. As to flexible TFSCs based on a-Si, they were more than 20 times cheaper [5]. And low costs determined the fast development of thin-film solar photovoltaics over the world. At that time I found my thesis very promising and possibly useful in the direction of combining the main challenges of increasing the PV efficiency in one solution (see. Fig. 1.1)

However, in 2011-2014 the price of mono-crystalline silicon reduced several times and became comparable with the price of other components

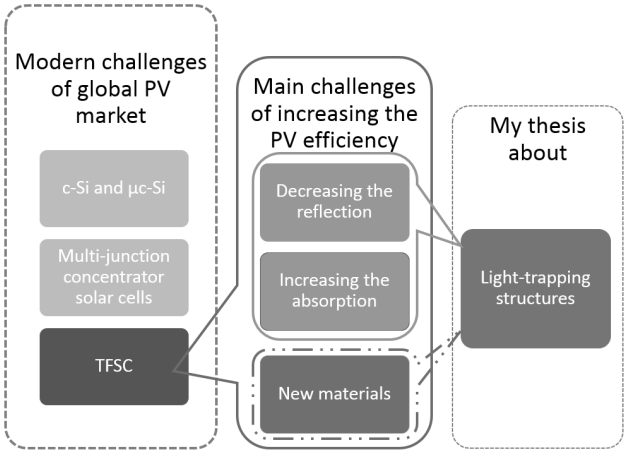

Figure 1.1. Schematic representation of the thesis location in the state-of-art context.

of a corresponding solar panel. It resulted from the ramp-up in the production of semiconductor devices for consumer electronics. In this period one started to manufacture silicon crystals for solar photovoltaic panels of the waste accompanying the fabrication of consumer electronics related to telecom applications. This manufacturing does not imply additional purification of Si. Toxic waste accompanying the fabrication of silicon SCs earlier vanished. In the same time, the cost of amorphous Si – basic photovoltaic material for industrially adapted TFSCs – also reduced similarly. The cost of a-Si is now negligibly small compared to the cost of other component of a solar panel. However, the cost of these other components – anti-reflective coating, current-collecting electrodes, metal contacts, circuitry for matching the solar panel to the useful load – kept the same. Therefore, the difference in prices per unit area of a monolithic SC based on c-Si and a TFSC based on a-Si has changed in favor of c-Si. This resulted in the crash of all companies specializing in thin-film solar photovoltaics. The crush held in 2014 over the whole world. Consequently, an amount of money allocated for research in this area reduced also over the world [8]. This situation could be foreseen and had been predicted in [9] 3 years before. Researchers explained how to avoid the collapse of thin-film photovoltaics, but the companies did not pay attention to this alert.

Well, does the industrial collapse of TFSCs mean that we have to stop scientific research in this field? No. The paradigm that "energy is needed where it is consumed" is still actual and will act in favor of the future development of TFSCs. The temporal crisis on the market of TFSCs does not mean the absence of the market prospective for them. TFSCs have sev-

eral principal advantages which will be listed below after the explanation of the operation principle and main features of TFSCs. These advantages have not crashed together with the companies, and the amount of scientific papers on TFSCs in the modern literature has not decreased since 2014.

In the potential market for solar photovoltaics the most volatile is that for rooftop electricity. The demand of this market implies detailed elaboration of issues related to the physical weight of the panels, their transportation, installation and the main ease of maintenance and replacement. These issues cannot be resolved without reducing the mass of the solar panel compared to the present design solutions of solar panels mainly targeted to high-power solar stations. The reduction of the mass is achievable only via the reduction of the thickness. Also, the conformal placement on the roof still requires the flexibility. Even nowadays, the market of TFSCs is not completely dead. It is waiting a pulse for a breakthrough. This breakthrough could be a drastic enhancement of the overall efficiency of TFSCs without the similar increase of their costs.

1.1.3 About PV diodes

Photovoltaic effect is conversion of a photon absorbed by a PV material, such as semiconductor, into a pair of two charges – electron with negative charge e and hole with positive charge $|e|$. The valence electrons in semiconductors can be excited to the conduction band in order to create mobile charge carriers. It is evident, that the minimal frequency of a photon that can be converted into the electron-hole pair is equal to that of the semiconductor bandgap ω_g – forbidden zone energy divided by Planck constant. To separate these charges creating the photocurrent is possible, for example, using the p-n junction. As it is commonly known from general physics, this junction results in a depletion region – lack of electrons at the n-doped side and lack of holes at the p-doped side of the junction. The depletion region has a very small thickness – typically few dozens of nm – that is identified with the effective thickness of the junction [1, 6]. So, depletion region as a double charged nanolayer and is characterized by a contact voltage that nearly equals $\hbar\omega_g/|e|$ [1, 5, 6]. This voltage represents a potential barrier for the photoinduced charges if the PV diode is illuminated but its contact are not connected to the external circuit. Open-circuit voltage of an ideal PV diode is equal to the contact voltage. In the open-circuit regime there is no electric field in the bulk of the diode.

Practically, by some reasons the open-circuit voltage is smaller than the contact one [6]. For a loaded diode this voltage drop results in Ohmic losses.

When the electrodes of the diode are shortcut the electric field extends to the bulk of the p- and n-doped parts and the corresponding voltages compensate the contact voltage. In the short-circuit case the equilibrium of Coulomb's attraction forces and repulsion forces resulting from the contact voltage in the depletion region is broken. Static electric field in the bulk of the photodiode move electrons and holes in the opposite directions, that results in the photoinduced current. This current flows oppositely to the direct current in the electrically open diode. In the short-circuit regime the photoinduced current is maximal and output voltage of the PV diode is nearly zero (the exact zero is prevented by finite Ohmic resistance of the diode). Usually, the term "photocurrent" refers namely to the short-circuit current [1, 6].

A proper choice of the load (i.e. matching of the PV diode to the external circuit) implies a deal between the maximal (open-circuit) voltage and maximal photoinduced current (short-circuit current) so that to maximize the power transferred to the load. In some PV diodes, i.e. those based on amorphous silicon (a-Si) the p-n junction is replaced by a heterojunction of p-i-n type. Such diodes are called pin-diodes. The minority charge carrier mobility in the doped a-Si is very low and their diffusion length is of the order of 100 nm. In the p-n diode of thickness 200 nm and more (when the thickness of p- and n-doped parts approaches or exceeds to 100 nm) the carriers of the photoinduced current thermalize and recombine before have attained the electrodes. This effect named the loss of charge carriers by recombination of electrons results in the heating of the diode by photoinduced charges. The p-n structure with doped layers thicker than the diffusion length is not a PV diode, it is a PV absorber. Consider the opposite situation – the p-n diode based on a-Si is much thinner than 200 nm. Then only a small part of the incident light will be absorbed in it because the optical decay in a-Si is not very high. A part of the sunlight power that can be absorbed in the PV layer but is not absorbed due to some reasons is called optical loss of the SC. So, for a p-n diode based on a-Si in one situation we have overcritical recombination losses, in the other situation – high optical loss.

In order to resolve this issue one reduces the thickness of the p- and n-doped parts do few dozens of nm and inserts a relatively thick intrinsic

a-Si part sandwiched between them. In this intrinsic sub-layer the main PV conversion occurs in photodiodes based on a-Si. Usually, the term "PV absorption" for photodiodes based on a-Si refers namely to the absorption in the intrinsic part of the PV layer. However, even in the intrinsic a-Si the diffusion length of electrons and holes is as small as one micron. Therefore, the optimal thickness of this sub-layer from the point of view of maximal photocurrent is nearly equal to 300-400 nm. Further decrease of this layer is not necessary because the cost of a-Si is very low and recombination loss it is also very low if the thickness is as small as 300 nm. On top of the p-i-n structure (illuminated by sunlight) the front electrode is located and on the bottom – the rear electrode. The total thickness of the whole structure including the top and bottom current-collecting electrodes does not exceed 1 micron and may be mechanically carried by a mm-thick flexible substrate. PV diodes based on a-Si and targeted to the solar energy conversion refer to the class of thin-film solar cells.

1.1.4 Solar cells as ultra-broadband PV diodes

Solar spectrum is ultra-broad, 5% of it occupies the ultraviolet range of wavelengths 300-400 nm, 43% – the visible range 400-700 nm and 52% the near-infrared range 700-2500 nm. But it is important to notice that the 90% of energy accumulated at the range of 380-740 nm. If the bandgap wavelength of a semiconductor of which the PV diode is prepared corresponds to 1800 nm, the PV conversion holds for the whole solar spectrum. This is a good point of the low bandgap. However, in this case too many absorbed photons have the excessive energy compared to $\hbar\omega_g$. When the conductive electron and hole in the photodiode move in opposite directions they spend their excessive energy $W_e = \hbar\omega - \hbar\omega_g$ to the thermal movement in the medium. This relaxation loss reduces the drift velocity of charges to the minimal value and the kinetic energy of the photocurrent carriers is much lower than the potential one. As a result, relaxation losses result in the decrease of both photocurrent in the shortcut regime and in output voltage in the loaded regime.

If ω_g corresponds to 1800 nm, W_e for wavelengths $\lambda = 320 - 500$ nm is much larger than the useful part of the photon absorbed energy $\hbar\omega_g$. It means that for such a low-bandgap semiconductor the dissipative losses are huge, that implies high parasitic (Ohmic) resistance of the PV layer and strong heating. The last effect is harmful – the dark current of a PV diode increases with the temperature and is opposite to the photocurrent.

It is clear that the bandgap of a semiconductor for solar photovoltaics should not be very high so that to minimize both useless sub-bandgap absorption and relaxation losses. From this point of view a-Si with its optimal $\lambda_g = 800$ nm is a very good material. However, as a PV diode it has drawbacks. One of them – insufficient absorption (low optical losses) – was already mentioned. Another drawback is rather low PV spectral response $SR(\omega)$ – factor that determines the internal quantum efficiency $SR(\omega)$ of a PV diode. Quantum efficiency gives the number of electrons output by the SC compared to the number of photons incident on the device, while the spectral response is the ratio of the current generated by the SC to the power incident on the SC. Internal quantum efficiency $IQE(\omega)$ is related to $SR(\omega)$ as

$$IQE(\omega) = \frac{\hbar\omega}{|e|} SR(\omega).$$

It does not take into account optical losses and is the property of the semiconductor. For example, for PV diodes based on a-Si it is the property of a-Si. In semiconductors with direct-bandgap $SR(\omega)$ is close to its idealization: $SR = \alpha\lambda$ if $\lambda < \lambda_g$ and $SR = 0$ if $\lambda > \lambda_g$. This proportionality results in the uniform quantum efficiency over the converted part of the solar spectrum.

For a-Si spectral response is a non-linear function of wavelength whose maximum corresponds to λ =600 nm. As the result $IQE(\omega)$ also has a pronounced maximum far from the bandgap. This results in lower integral power of converted solar spectrum compared to GaAs, CdTe, and other direct-bandgap semiconductors. Amorphous silicon also does not stand comparison with best indirect bandgap semiconductors, such as c-Si. The PV spectral response of a-Si at its maximum is only slightly lower than the maximum of $SR(\omega)$ for c-Si. However, the sub-band radiation losses are higher due to shorter bandgap wavelength (800 nm against 1050 nm for c-Si). Therefore, the overall efficiency of an idealized (no optical losses and negligible resistive losses) SC based on a-Si is almost twice lower as the overall efficiency of an idealized SC based on c-Si [11]. The last drawback of a-Si SCs is nearly 30% degradation of the efficiency after a long solar exposure. This degradation is called Staebler-Wronsky effect [6] and its physics is still disputable [8].

However, if we compare a-Si with other amorphous PV materials (except perovskites, that we will discuss below separately) a-Si gains in the spectral response compared to them. Also, it has tunable bandgap – tunability

in the range 1.7 ± 0.1 eV (λ =690-770 nm) is offered by hydrogenization. Also its Fermi level may be controlled by doping, as phosphorous for the n-type materials and boron for the p-type [6]. The tunability of a-Si enables the optimization with different materials of electrodes so that the Ohmic loss can be minimized and the open-circuit voltage can be kept practically equal to the contact voltage. This allows the TFSCs based on a-Si to be a potential competitor to silicon solar photovoltaics. The lack of efficiency (compare to SCs on c-Si) and 30% degradation after a durable solar exposure (that hopefully will be eliminated in the near future) are compensated by such advantages as low production costs, low weight, absence of production waste and flexibility. The last one allows the conformal placement of SC on waved surfaces such as the roofs, integration with clothes and even with human skin (see below).

1.1.5 Optical efficiency of thin-film solar cells

Optical absorption in a-Si is not very high. Even 400 nm of thickness for the intrinsic sub-layer is not enough in order to absorb the whole incident light per one passage across the PV diode. If the total thickness of the p-i-n structure of a-Si is equal to 500 nm (50 nm for hydrogen-doped sub-layers with optimal carrier concentration (usually $1 \ldots 3 \cdot 10^{18}\, 1/cm^3$) and 400 nm for the intrinsic sub-layer), the absorbance of light with wavelengths 600-800 nm (slightly shorter than the effective[1] bandgap wavelength of intrinsic a-Si λ_g =800 nm) in the PV layer is close to 50% [13]. For a-Si photodiodes whose PV layer is optimized so that to attain the maximal current and minimal Ohmic losses the transmission losses exceed 50%. These losses arise because in these TFSCs, the bottom electrode is not a reflector performed of a polished metal. Such electrode can be an Al foil whose Ohmic contact with the semiconductor is ensured by a conductive paste. Alternatively, it can be a transparent conductive oxide (TCO) or other transparent conductive material – the same of which the top electrode of the SC is prepared. For both these design solutions the light transmitted through the PV layer must be dissipated.

For thin flexible PV diodes the transmission optical losses become a critical harmful factor [8]. Therefore, companies that produced a-Si SCs before 2014 preferred to sacrifice the low-level of recombination losses in favor of high optical efficiency and fabricated their TFSC with intention-

[1] Amorphous silicon has no direct bandgap, its band structure is different from that of c-Si.

ally increased thickness of the PV layer. In [7] it is asserted that a one micron thick p-i-n structure is the best choice for the a-Si SC on a flexible substrate, because it allows the angle-averaged optical efficiency higher than 80%.

For such TFSCs the situation with optical efficiency is the same as for usual SCs having optically thick PB layers such as wafer SCs. Optical losses are practically equal to the reflection losses. The reflection losses of a bare SC averaged over the daytime are as high as 35-40% or even higher. If the collection of the photocurrent from the top interface of the PV layer is performed by a mesh of wires, nearly 10% of light is reflected by these wires. This reflection loss corresponds to the shadowed area where the reflection is total because the metal is not transparent. This reflection cannot be reduced. However, in the mm-sized gaps between the wires the top surface of such the PV diode is that of a semiconductor – a material with high refractive index ($3.5 - 4$ and even more). This implies a high reflection also in the mm-scale gaps between the current-collecting wires. And this reflection can be reduced by a layered structure called anti-reflective coating (ARC).

Alternatively, the top electrode can be performed as a layer of a transparent conducting material. Then there is no shadowed region[2]. However, the reflection of solar light in absence of the ARC keeps high. Transparent conducting materials have the refractive index close to 2, that implies a significant optical contrast with both free space [3] and semiconductor. As a result of this optical contrast the reflection arises at both interfaces of the transparent top electrode and contributes into the total reflection. After averaging over the daytime incidence angles the integral reflection loss of the bare TFSC based on a-Si with a transparent top electrode turns out to be slightly (5-7%) lower than that corresponding to the SC with a wire mesh. And this slight advantage is compensated by the optical loss in the transparent electrode. Really, a static conductivity is not possible for a completely lossless materials. Only in dielectrics the optical losses are negligibly small. For transparent conductive oxides the complex permittivity in the optical range has a rather noticeable imaginary part of the order of 10^{-3}. And a typical thickness of the transparent electrode cannot

[2]More exactly the shadowed region still exists because there are contacts wires in order to connect the top electrode to the external circuit but their shadow can be made negligibly small.

[3]In fact, a practical SC is covered by a laminate of macroscopic thickness protecting the SC from the abrasion in the Earth atmosphere. However, the refractive index of usable laminates is in the range $1.34 - 1.38$ i.e. close to that of free space.

be very small, otherwise the electrode brings high ohmic losses. As a result, there is no noticeable difference in optical losses inherent to TFSCs with a TCO layer and to TFSCs with a wire mesh.

To reduce the reflection losses to acceptable values anti-reflective coatings (ARCs) are used. In some exotic SCs, multilayer ARCs are used. They comprise from 4 to 12 nanolayers performed with nanometer precision and allow decreasing the integrated reflection in the whole sunlight spectral range down to 1%. Of course, such coatings are very expensive and not suitable for SCs used in everyday situations. They are used in multijunction SCs and GaAs SCs. We do not concern such SCs in this thesis. Though multijunction SCs are very efficient (overall efficiency for normally incident light attains 38%) they are also very expensive and, therefore, used mainly on satellites [1]. As to GaAs SCs – they are also more efficient than SCs based on c-Si, but their PV material is much more expensive and the waste accompanying its production is very toxic [5]. Moreover, multilayer ARCs applied to such SCs though are excellent for the normal incidence lose their advantage for large incidence angles. Their use is justified only if the solar panel rotates after the sun. This complication is only acceptable for solar panels dedicated for mass production of electricity in the solar power parks. Moreover for such panels the crystalline silicon still has no valid counterparts [5].

As to TFSCs, the paradigm of cheap solar electricity for domestic and mobile usage implies that the ARC must be as cheap as the SC itself. It means that a one-layer ARC should be used. It order to achieve the wide-angle suppression of reflection one suggested a composite ARC realized as a dielectric film with random arrays of sub-micron inclusions [10]. It can be also a monolayer of densely-packed dielectric particles on top of the structure (see below).

However, for TFSCs based on a-Si, the advantages of these design solutions (offering few additional percents of reduction for the angle-averaged reflection coefficient compared to a flat dielectric nanolayer) are not principal. For such SCs the ARC performed as a nanolayer of SiN (wire mesh) or silica (transparent electrode) resolves the problem of reflection losses. Notice, that in TFSCs based on a-Si the top electrode is most often performed of flexible transparent conductive material with nanometer precision and the whole structure is already a multilayer with rather high optical contrast. Reflection losses of a bare TFSC for normal incidence do not exceed 15-20%, and the use of an affordable ARC performed as a

nanolayer of SiN or silica reduce them to few percents. For the daytime-averaged reflection losses a flat one-layer ARC offers the reduction of reflection losses from 35-40% to acceptable 15-17% [10].

However, for flexible a-Si TFSCs, the utilization of ARCs does not resolve the problem of high losses. If we increase the thickness of the PV from its optimal values 300-400 nm to 1 micron as it was reported in [7], we substitute the transmission optical losses by the increased recombination losses. Then the result for the overall efficiency is the same 4.5% [7]. If we reduce the recombination losses to the minimum choosing the optimal thickness of the PV layer an ideal ARC basically replaces the reflection losses by the transmission losses. In both cases the result for the overall efficiency is within the same pitiful 4-5%. Moreover, in the second case the dissipation of sunlight in the bottom electrode results in its heating. It can be harmful for the substrate and one has to take care about cooling such the SC. This is the reason why the industry preferred to use micron-thick p-i-n structures.

In order to prevent the parasitic transmission keeping the optimal thickness of the p-i-n structure, one needs to substitute (complement) an ARC by a special structure would trap the light inside the PV layer preventing its propagation downward. Such passive structures are called light-trapping structures (LTSs). The target for an LTS is to suppress both reflection and parasitic transmission. To have a commercial perspective LTSs should be efficient in the ultra-broad spectrum of wavelength, in the wide spectrum of incidence angles and to be inexpensive. This is a challenging but feasible task.

Creation of LTSs for TFSCs became actual in early 2000s. Hundreds of LTSs for a-Si TFSCs have been suggested since that time (see in overview [8]) and leading scientific journals continue to publish corresponding papers [12–14]. Most of these LTSs represented nanostructures of plasmonic metals, some of them are arrays of dielectric/semiconductor nanoparticles. However, no one of these design solutions was, to our knowledge, industrially adapted. And it is not surprising. Since the light-trapping was achieved due to the involvement of evanescent waves, high-order spatial harmonics of regular LTSs and/or resonator modes of nanocavities the successful operation of these structures implied strict fabrication tolerances and nanometer spatial resolution. This made such LTSs too expensive for mass production. Second, many authors did not apply their LTSs to truly optimal TFSCs. In order to stress the advantages of their

LTSs they made the p-i-n structure thinner than 300 nm demonstrating the positive impact of their LTSs by price of reduced overall efficiency. This approach is harmful for the idea of a light trapping structure as a promising alternative to an anti-reflecting coating (ARC).

1.1.6 Advantages and disadvantages of thin-film solar cells

Let us sum up advantages and disadvantages of TFSCs based on a-Si compared to c-Si. Advantages are as follows:

- lower cost;
- practically no waste accompanying production;
- lighter weight;
- possible flexibility;

Disadvantages are as follows:

- lower efficiency;
- Wronsky-Staebler degradation.

Here one advantage and one disadvantage mentioned first have key importance for the future of thin-film photovoltaics based on a-Si (Wronsky-Staebler degradation is, to our opinion, an important but not a vital issue for TFSCs).

Currently, the price per square meter of commercially available silicon solar panels is only twice higher than that of a-Si TFSCs. This difference is insufficient so that to compensate the lack of efficiency of TFSCs. However, on condition of sufficient demand the roll-to-roll fabrication of flexible TFSCs will grant much lower prices per square meter [7]. Next, currently the overall efficiency of industrially adapted a-Si TFSCs on flexible substrates is nearly 4 times lower than that of silicon SCs. The reason is transmission losses in TFSCs having the optimal thickness of the PV layer. In industrially adapted TFSCs the transmission losses are absent but substituted by recombination losses (the PV layer is taken much thicker than its optimum). On condition of the successful commercializing of new LTSs suggested below, in this thesis, the optical efficiency of TFSCs higher than 80-90% can be achieved for the whole daytime. This high optical efficiency can be obtained for TFSCs having the PV layer of optimal thickness 300-400 nm.

If the optical efficiency grows twice compared to that achieved nowadays for a-Si TFSCs with optimal deisgn parameters, the overall efficiency will also duplicate. Then the overall efficiency of a-Si TFSCs will be still lower than that of silicon SCs, but lower only twice and not four times. And if this increase of the efficiency is not accompanied by the increase of the cost, the twice lower efficiency will corresponds to the twice lower price. If the ratio efficiency/cost is the same for both counterparts, such advantages of the thin-film photovoltaics as low weight and flexibility will overturn the present situation. Thin-film photovoltaics will get a strong pulse and will, most probably, gain the contest with the crystalline silicon for ever.

1.1.7 Excitonic PV devices and perovskite solar cells

As well as SC based on a-Si excitonic PV cells are also intrinsically TFSCs. Though exitonic solar cells have not been commercialized, yet, they seem to be promising. The most popular design of an exitonic SC with flat heterojunctions comprises a nanolayer of organic polymer named donor located on the bottom electrode and coated with a nanolayer of transparent material having the electron type conductivity named acceptor. A transparent electrode is located on the acceptor. In both nanolayers – donor and acceptor – solar light generates a specific electron-hole pair called exciton. The difference of the exciton from a usual electron-hole pair is the high energy of coupling. High potential energy implies high quasi-static field in the exciton. At the interface of the donor and acceptor layers excitons split onto free electrons and holes. This dissociation results in the photoinduced current if such the PV device is loaded by a finite impedance or is shortcut. Excitons have the finite lifetime and their diffusion length is of the order of 100-200 nm. Since excitons that do not achieve the boundary recombine and do not participate in the photocurrent, the thickness of the PV material is such SCs must be essentially submicron.

Metal-organic perovskite SCs are also referred by many authors as exitonic PV devices, however, to our opinion they deserve to be classified separately. The hottest topic in the literature of modern solar cells is namely the field of metal-organic perovskite SCs. Since 2014 the dominant literature on TFSCs has referred namely to perovskite SCs.

Perovskite crystals were revealed in nature and described by V. Goldschmidt in 1926 [16]. Recently one created artificial metal-organic analogues of natural perovskite crystals. Perovskites have polycrystal struc-

ture with several lattices of micron and even sub-micron areas that can be within one domain coordinated in different crystal planes. This makes perovskite compounds mechanically amorphous. Metal-organic perovskites are very cheap synthetic materials that possess a high optical absorption in the visible range and a surprisingly high internal quantum efficiency (at least in few days after fabrication). This makes them promising for flexible thin-film photovoltaics [52]. In perovskite TFSCs the generation of excitons occurs in the central layer typically sandwiched between the electron-conducting and hole-conducting nanolayers. However, due to a rather high dielectric constant of a typical 3D perovskite, the exciton binding in it is much smaller than in an organic material. This central layer has also an essentially submicron thickness and namely the central layer is performed of a perovskite compound.

The best samples of such SCs before the degradation of their constitutive materials exhibit the overall efficiency as high as 20% and even more. The record for these TFSCs exceeds 30% [8]. Even produced in the university laboratory perovskite SCs are very cheap. The main problem with these SCs is a low stability of material properties that will be probably resolved with the creation of a reliable and non-damaging encapsulation technique. Also, the issue of flexibility for such TFSCs is not completely resolved [8]. However, first promising results for flexible perovskite SCs were obtained – the efficiency 15.6% was recently reported in work [17]. We hope that the problems hindering the commercialization of perovskite SCs will be resolved in the near future. Therefore, in the theoretical part of this thesis there is a chapter about perovskite SCs.

1.2 Light-trapping for thin-film solar cells

For hard TFSCs such as TFSCs based on epitaxial silicon the problem of possible increasing the optical absorption is resolved utilizing ARCs and surface texturing by pyramids or prisms with typical sizes of few microns. This texturing has been known since 1970s (see e.g. in [8]). If the sunlight impinges the textured surface normally, it enters into the PV layer obliquely and then reflects from the polished back electrode. Then its strongly tilted path is sufficient for a total absorption of light. Texturing the surfaces in this way is often referred as light trapping, though in our terminology such TFSCs have no LTSs.

We need to trap the light incident on a surface that is flat in the scale

of the light wavelength. A good LTS for our non-textured TFSCs should reduce the parasitic transmittance without increasing the reflectance. If it is located on top of the TFSC it should also perform the antireflective functionality. This enhancement of optical efficiency must be achieved without a drastic increase of the fabrication cost. This task became a key issue of thin-film photovoltaics based on a-Si since its commercial start in early 2000 [11].

The majority of works in the field of LTSs for TFSCs corresponds to two approaches: so-called plasmonic LTSs and so-called photonic crystal LTSs. Numerous plasmonic LTSs were suggested for a-Si TFSCs and photonic crystal LTSs – for TFSCs based on poly-crystalline Si (see e.g. in [20–27]). We do not aim to review this literature. For our purposes it is enough to mention general drawbacks of all these structures. Photonic crystals embedded into a TFSC are regular nanostructures obtained by electron or ion beam lithography (in rare cases by nanoimprint lithography). They are expensive structures, whose cost is hardly compatible with the idea of cheap solar electricity. Let's concentrate on more affordable LTSs.

In the dominant literature of LTSs for a-Si TFSCs the increase of the optical efficiency granted by the LTS is claimed. This is hardly relevant because bare TFSCs – without ARCs – are not practically used. In order to properly describe the advantage granted by an LTS the optical efficiency of the SC enhanced by this LTS must be compared with that of the SC enhanced by a typical ARC.

I have mentioned above that a typical ARC for TFSCs based on a-Si and utilizing the transparent top electrode (TCO) is a simple nanolayer. The material of this layer has refractive index whose value would be in the middle between unity (that of free space) and that of the TCO. For TFSCs based on a-Si the top electrode is often performed of aluminium-doped zinc oxide (AZO) or indium-tin oxide (ITO) having the refractive index close to 2. In this case the suitable material for ARC is silica. Notice, that if the top electrode is fabricated of silver nanowire network [18] or network of carbon nanotubes [19] whose refractive indices are close to 1.6 the ARC is not required – its role is played by the transparent electrode itself [18, 19].

However, the fabrication of such electrodes is, for the present time, possible only in few scientific groups, and the question of costs for mass production is not clear, yet. We will compare our LTSs with typical ARCs of silica and silicon nitride. Such materials have a suitable refractive index and allow the ARC to be fabricated with the nanometer precision us-

ing the standard and cheap technique called plasma-enchanced chemical vapour deposition. We have already mentioned that a so simple ARC with optimized thickness reduces the angle-averaged reflection losses from 35-40% to 15%. Our LTSs may yield a little to the ARCs in the anti-reflective operation. Then this disadvantage must be overcompensated by the reduction of transmission losses so that the LTS is advantageous compared to the ARC.

1.2.1 Resonant light-trapping structures

Plasmonic LTSs (see e.g. [25]) are affordable if they are metal island films – random arrays of nanoislands of silver or gold on top interface of he PV layer or on its bottom interface. Such amorphous structures can be grown chemically. Their location on the top interface is hardly reasonable because metal elements of the surface increase the reflection. However, even their location on the bottom interface between the PV layer and the bottom electrode has an inherent drawback. Metal island films possess inherent resonant losses at the plasmon resonances. These losses occur namely in the metal elements: the region of the resonant local field enhancement called plasmonic hot spot cannot be fully eliminated from the metal. In practice, in such LTSs transmission losses in the bottom electrode are substituted by similar losses in their own. It is not surprising that no one of known irregular plasmonic LTSs gives an enhancement compared to that offered by a usual ARCs [8].

A noticeable enhancement can be obtained using regular structures of gold or silver nanoelements. These regular arrays when located beneath the PV layer or incorporated into it can mimic an effective optical facet converting the incident plane wave into eigenmodes propagating in the PV layer as in the waveguide [25, 28]. Here it worth to note that usual phased optical gratings serving in the integral optics to the same purpose – conversion of the incident wave into a waveguide mode (this is how nowadays flat optical waveguides are connected to external optical circuits) are inefficient for a-Si TFSCs. The reason is the strongly submicron thickness of the PV layer, much smaller than the height of a teeth of the optical facet. This smallness makes the excitation of the waveguide mode by the grating inefficient. The functionality of the phase grating is performed by the regular plasmonic grating [8].

Alternatively, a regular array of specially designed metal nanoelements may convert the plane wave into collective oscillations of the array itself.

These modes are located on the frequency axis rather far from the plasmon resonances of individual metal elements. Plasmonic hot spots are located in the gaps between the elements and parasitic losses in the metal turn out to be much lower than those inherent to island films [29, 30].

At a first glance, these advantageous regimes make regular plasmonic LTSs promising for the enhancement of TFSCs. However, for a-Si solar photovoltaics dedicated for the mass production and consumption it is apparently not so. Regular arrays of metal nanoelements obviously imply high fabrication costs, and their market prospectives are as doubtful as the future of LTSs based on photonic crystals.

Recently, all-dielectric LTSs exploiting different kinds of resonances in an array of dielectric spheres (whispering gallery resonance, magnetic Mie resonance, combination of these resonances, and spatial resonance of a photonic crystal of dielectric spheres) have been suggested for a-Si TFSCs. These arrays are located on top of the SC. In accordance to works [31, 48] they combine the light-trapping and anti-reflective functionalities being densely packed. In view of commercially available micron and submicron dielectric spheres, including quartz and silicon ones, and possibility to pack them densely in a very simple way (see below) these structures seem to be promising for commercialization. However their resonant behavior implies a narrow frequency range for the light trapping effect. Therefore, they grant a only very modest (2-3%) increase of the useful absorption compared to a flat ARC even for the normal incidence. Their behavior for oblique incidence was not studied in cited works. However, the resonances of these ARC keep the same narrowband effects for large incidence angles as they are for the normal incidence. In this thesis we aim a much more significant suppression of the parasitic transmittance in TFSCs than that granted by resonant dielectric LTSs, known to the present time.

The key issue for a-Si solar photovoltaics is to approach to the overall power conversion efficiency of an idealized SCs based on amorphous silicon (15-16%). Practically, for flexible TFSCs one has to achieve, at least, 10% of the overall efficiency. And this target seems to be achievable.

At least, for TFSCs employing the bottom electrode of polished metal such the efficiency has been already demonstrated. Namely, the overall efficiency 10.2% was obtained (for the normal incidence) in a TFSC comprising a 310-nm thick p-i-n structure and a hard bottom electrode of polished silver [15]. In this structure, an ARC of silica was used and

the optical efficiency for the normal incidence exceeded 90%. This record was achieved without any LTS because in this case the light is reflected by the bottom electrode and not lost in it. This internally reflected light is almost fully absorbed during its second passage through the 310 nm thick PV layer.

However, for industrially adapted a-Si TFSCs with flexible substrates the overall efficiency is still as low as 4-5% because of half of the incident light is absorbed in the bottom electrode and no one of numerous suggested LTS has been industrially adapted. Meanwhile, the flexibility is the key point of the amorphous solar photovoltaics, it is the feature making this industry potentially attractive for customers. This is why the amorphous silicon solar photovoltaic industry has declined and is presently fully substituted by the photovoltaics based on c-Si.

If it only were possible to obtain 10% for flexible a-Si TFSCs, this would give a strong pulse to this stagnating branch of photovoltaics. And what is the key obstacle in the approach to the targeted 10% for flexible a-Si TFSCs? High level of transmission losses in the case of 300-400 nm thick PV layers (or high level of recombination losses for an intentionally increased PV layer). Light-trapping structures is the tool to eliminate the transmission losses for TFSCs with PV layers having 300-400 nm thickness? All we need is to develop LTSs which would deserve commercialization rather than publication in high-level scientific journals.

The main achievement described in this thesis is creation of such novel LTSs.

1.2.2 What is my thesis about

The main goal of my thesis is achieved involving non-resonant matematerials. However, some partial goals are targeted by resonant ones. Metamaterials (MMs) are artificial media with extreme electromagnetic properties not achievable in natural media and advantageous for applications. Most part of MMs are performed of resonant constituents and our original research starts namely from a resonant MM.

In the next chapter of this thesis we report the study of a-Si PV diodes illuminated by a rather narrow-band light. In this case we do not need an ultra-broadband operation. We will theoretically show that an affordable plasmonic MM incorporated into the PV layer grants a significant enhancement to the PV absorption. Further, we will theoretically study a perovskite PV diode operating as a TFSC. It will be also enhanced by

a similar resonant MM. It is possible because the issue of transmission losses arises for perovskite TFSCs only in a narrow frequency band. Advantageous properties of these narrow-band LTSs and their affordable fabrication technique, to my opinion, make them promising for commercialization, at least more promising than their previously known counterparts. This part of the thesis is purely theoretical.

The most important part of this thesis is targeted to a-Si TFSCs. These potentially high-efficiency flexible TFSCs required of us very broadband, easily feasible and cheap design solutions. We have found these solutions introducing two types of non-resonant light-trapping MMs. These novel design solutions are theoretically and experimentally studied in two last chapters of this thesis. Their fabrication refers to cheapest types of known micro- and nanotechnologies. Meanwhile, we have shown the unprecedent enhancement of the useful optical absorption granted by such LTSs to a-Si TFSCs with nearly optimal thicknesses of the PV layer (400-500 nm). Therefore, I believe that my doctoral research deserves attention of innovators.

1.3 Micro- and nanotechnologies in the fabrication of light-trapping structures

It is worth to mention that the most part of the experimental work, including fabrication of all samples, has been done in Micronova – Micro- and Nanofabrication center of Aalto University. My fabrication methods were Physical Vapor Deposition(PVD), Reactive Ion Etching (RIE), Ion Beam Etching (IBE), Atomic layer deposition(ALD), Plasma-Enhanced Chemical Vapor Deposition(PECVD), and Optical Lithography (OL).

Of course, the development of methods for nano-patterning and nanotexturing electron and ion beam lithography start a new era of metamaterials (e.g. [36]). Developing of new etching and deposition methods (like Laser Induced Deposition) open new doors for textured thin films and allow us to produce nanoantennas [50] and other metallic nanoparticles [51].

However, in the present thesis only affordable, potentially attractive for mass production methods of fabrication will be used. To our opinion, ALD also refers to affordable techniques. Currently, ALD is still considered as an expensive method and is considered as that offering us the possibility to create exotic nanostructures. One of them is shown in Fig. 1.2.

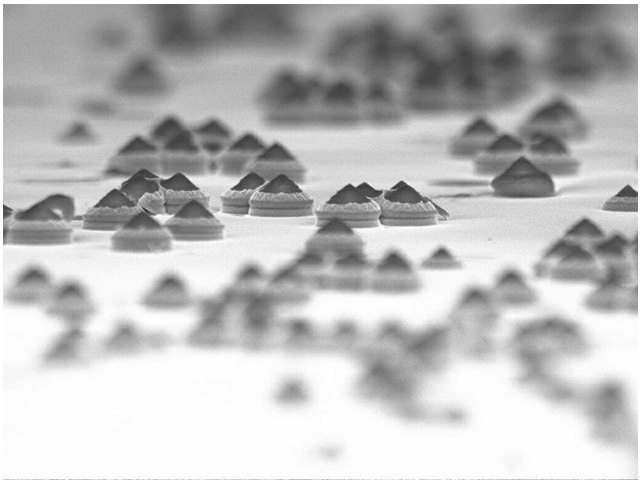

Figure 1.2. Artistic reproduction of a traditional African village in the submicron world.

This nanostructure is a billion times reduced copy of an African village. I have fabricated it utilizing the ALD and IBE techniques. Of course, production of such nanometer-scale textures is expensive because it is very time-consuming. However, all we need from ALD for producing a-Si TFSCs enhanced by our LTSs is uniform deposition of atoms up to a certain thickness, e.g. 500 nm. In this situation ALD can be a potentially cheap technology. Its perspective for the mass production of sub-micron layers with nanometer precision as it is explained in work [37] are very favorable. In accordance to this work, ALD will enable the mass production of TFSCs with transparent top electrodes performing the anti-reflective functionality.

In this section I concern only the standard techniques. Some original techniques I have used for fabricating the experimental samples (such as self-assembly of colloidal particles into a densely-packed monolayer) will be discussed below.

2. Plasmonic Metamaterial for Enhancement of a-Si Photodiodes

2.1 Metal nanoparticles for absorption outside the metal

2.1.1 Biomedical application of a-Si photodiodes

Not only SCs can be PV generators, electricity can be produced by a photodiode illuminated by a lamp which is named artificial light and has to deliver the main energy at totally different wavelenght compare to the natural (solar) light. We found in the literature a set of devices, called biomedical chips, for which flexible PV cells operating in an artificial light are required. Such structures can be, for example, applied on top of the chips and serve electric generators. In accordance to [40], a PV diode located on top of this chip (integrated with human's skin) will play the role of the presently used battery feeding the chip. The power will be harvested by a flexible thin-film PV cell (serving also a laminate for the chip) from an artificial light collimated on it. For this devices the whole PV diode and LTSs can be rather narrowband if the light source is a lamp producing a light of certain color. It may operate also in the infrared range if the source is an IR lamp or IR light-emitting diode. A typical bandwidth of such devices does not exceed 10% of solar spectre. Assuming that the PV diode for this application should be cheap, we suggest for this purpose a narrow-band analogue of an a-Si TFSC on a flexible substrate with a TCO top electrode.

The PV absorption in this narrow-band PV diode is enhanced by a resonant LTS that should be integrated with the PV cell. Here we exploit a novel regime of perfect absorbtion granted to the host material by a plasmonic metamaterial incorporated into it. The frequency-selective enhancement of the useful absorption occurs so that the parasitic absorption

in the metal is very small. This regime corresponds to a novel mode of a planar array of densely arranged plasmonic nanospheres. This regime holds for both metal-backed variant of the PV cell and with its semitransparent variant (transparent bottom electrode and dielectric substrate as a mechanical carrier of the structure).

The key point here is how affordable will be such the LTS. If the fabrication costs of our LTS are assumed to be much higher than the cost of the reference TFSC, our suggestion is practically useless. Fortunately, we see the possibility of affordable fabrication of our LTS. This point is discussed in the end of the Chapter.

2.1.2 Plasmonic perfect absorber operating as Huygens' metasurface

This novel regime was theoretically revealed in [38] for a sub-wavelength thin highly-refractive layer with incorporated silver nanospheres. This layer depicted in Fig. 2.1 was called in [38] Huygens' metasurface. It is an optically thin composite layer formed by densely arranged plasmonic nanospheres. Optically dense arrays of resonant elements represent the most common class of MMs, and 2D – monolayer – arrays are often called metasurfaces. As to the name of Christiaan Huygens, it comes from the peculiarity of the operation of our MM.

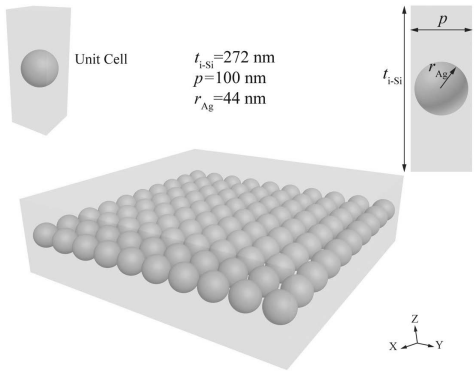

Figure 2.1. Amorphous silicon layer with symmetrically located grid of densely packed plasmonic nanospheres and the unit cell of the structure.

At the resonant frequency the backward scattering of silver nanospheres exactly compensates the reflection from the hosting layer. The latter is rather high – though its thickness is subwavelength, the refractive index is assumed to be rather high (of the order of 2 or higher). Since the reflection coefficient of our MM layer is zero, and the transmittance in the lossless case is unity, the unit cell of the MM can be treated as a Huygens'

element. Huygens' element is a pair of orthogonal electric and magnetic dipoles equal to one another (after a normalization by the wave impedance of free space). This pair in the Huygens theory of diffraction mimics an element of the wave front.

Notice, that the Huygens' regime for diffraction grids is also called Kerker's effect and the MM of work [38] due to its periodicity can be also referred as Kerker's diffraction grid operating at a low frequency (much lower than the frequency at which diffraction maxima arise).

Now, let us mention the main result of [38]. It is as twofold. First, if optical losses in silver are taken into account but the host material of the layer is lossless the resonant transmittance is still almost equal unity. It can be so only if the absorption in our silver spheres is very low. This statement was confirmed in [38] by the analysis of the local field distribution. It shows that plasmonic hot spots are located beyond the silver spheres.

Second, if the material of the layer is lossy, the reflection keeps zero but is complemented by strong absorption in the layer. Concentration of the electric field in plasmonic hot spots located inside the lossy material strongly increases the absorption. Therefore, the transmitted wave in presence of nanospheres experiences a much higher decay than a plane wave in a host material without nanospheres. Then absorption is perfect and this is absorption holds not in silver.

This unusual property can be used for the enhancement of the PV absorption if the plasmonic nanospheres are incorporated into the intrinsic layer of a a-Si photodiode. Therefore, in the reported study we transit from the uniform host to a p-i-n structure of a-Si PV diodes. In this study we assumed that the array is formed by Ag nanoparticles. We changed the diameter in the band 80-100 nm. This variation changes the resonance frequency in the same relative interval ($\pm 10\%$). A 30-nm thick layer of p-doped a-Si is on top of the structure and a 25-nm thick heavily n-doped (density of majority carriers 10^{20} 1/cm^3) layer of a-Si is on the bottom. The last is practically a part of the bottom electrode. It can be terminated by a metal layer or a layer of transparent conductive material. We have simulated both these structures. In the first one the ohmic contact of n-doped a-Si with the Al foil requires a sublayer of chromium with typical thickness 5 nm. In the second version the n-doped layer is terminated by a 100 nm thick AZO layer on the organic glass substrate.

In spite of high optical decay inherent to the bottom layer the useful

regime with dominant PV absorption in the intrinsic a-Si survives. In the band of the resonant absorption the wave does not attain the n-doped layer and is almost fully trapped in the intrinsic silicon. At the operation frequency the parasitic loss in Ag is as small as 4%, whereas parasitic loss in the bottom layer of n-doped silicon is much less than 1%. As to the absorption in the p-layer, it is not desirable due to higher recombination loss in the doped a-Si than that in the intrinsic a-Si. But this absorption also contributes into photocurrent – the spectral PV response of the p-doped a-Si (density of majority carriers 10^{18} 1/cm^3) is quite substantial [1].

In spite of these changes we have managed to engineer the same Huygens' regime as was achieved in [38] for a MM grating incorporated into a bare 400 nm layer of a-Si. We have implemented the same resonant absorption in the intrinsic a-Si, but now this layer is a part of a realistic PV diode with optimal thicknesses of all sublayers (see Fig. 2.2). The presence of the front transparent electrode and the p-doped a-Si sublayer on top of the intrinsic layer and the presence of the heavily doped a-Si sublayer with the rear electrode on the bottom of the intrinsic layer shifts the operation frequency (from 500 THz to 510 THz) and slightly changes the optimal geometric parameters of the array. But the effect survives as such.

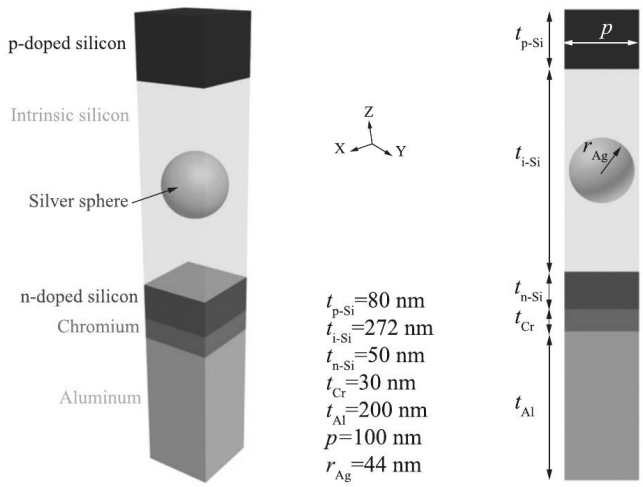

Figure 2.2. The PIN structure with Ag spheres in the intrinsic a-Si.

Thus, a perfect plasmonic absorber operating as a Huygens' metasurface is suggested for the enhancement of the PV absorption in a PV diode. Definitely, this idea has been suggested for the first time since this absorption regime was theoretically revealed namely in our Department and my

supervisor and I participated in the first paper describing this regime – work [38].

Of course, perfect plasmonic absorbers were known before. However, they operated very differently. Previously known perfect plasmonic absorber were implemented as a plasmonic MM – a planar array of plasmonic elements (nanospheres, nanodiscks, etc.) located at a small distance from the metal or doped semiconductor substrate [41–44]. This distance is offered by a few nanometer thick dielectric spacer.

In this structure the resonant optical absorption is offered by polarization currents that flow in the substrate in one direction and in the plasmonic array – in the opposite direction. More exactly, this opposite polarization of the plasmonic elements corresponds to the magnetic mode of the MM, and the resonant absorption is achieved when the dipole mode (polarization currents in the substrate and in the array flow in the same direction) and the magnetic mode are balanced.

This regime is not advantageous for application in the PV diode purposes. In previously known perfect plasmonic absorbers at least one half of absorbed power is absorbed in the metal nanoparticles. Our target is to increase only the PV absorption and to get rid of the absorption in the metal.

To be frank, we have to mention that the resonant perfect absorption without parasitic absorption in the metal also had been known prior to publication of our paper [38]. In works [45, 46] one suggested to exploit the magnetic Mie resonances of Si nanoparticles shaped as tablets and located on the semiconductor interface. We have inspected the possibility to apply this structure for the enhancement of a-Si photodiodes and concluded that we did not see an affordable technique that would allow one to implement it incorporated into a PV diode. The structures reported in [45, 46] are interesting for scientific laboratories and hardly for mass production. As to our structure, we know how to fabricate it in the affordable way. Therefore, in our future studies in this chapter we exploit the regime revealed in [38].

2.2 Local field concentration and enhancement of useful absorption

The local field concentration in our PV diode with the transparent rear electrode at the resonance of absorption (510 THz) is illustrated by the

electric field color map of Fig. 2.3. Polarization current density in the bulk of the unit cell depicted in Fig. 2.3 is proportional to **E** with the coefficient $i\omega(\varepsilon - 1)$ (where ε is the permittivitty of the material at the observation point). At this frequency the absorption attains 97%.

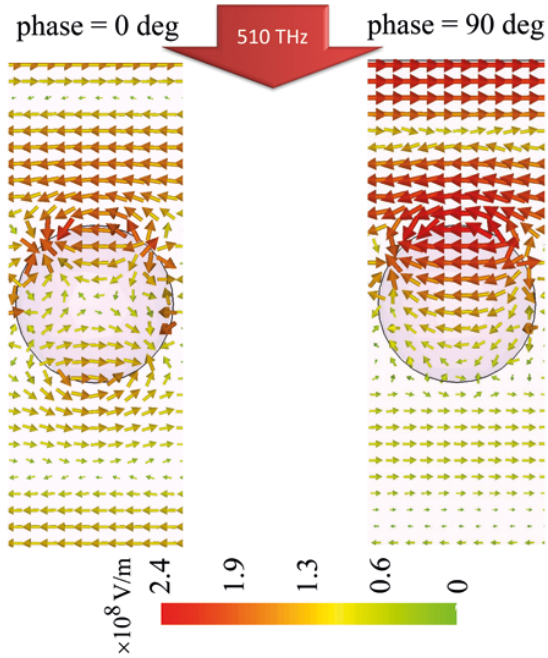

Figure 2.3. Electric field distribution in the unit cell our metamaterial at the frequency 510 THz for two time moments shifted by one quarter of the period. The case of Ag spheres of diameter 90 nm.

Two color maps in Fig. 2.3 are simulated for two time moments shifted by a quarter of the period from one another. Though **E** concentrated in the top half of the layer is polarized nearly horizontally, it is not the field of a plane wave transmitted into a-Si. First, vectors **E** change their direction to the opposite one so that the planes of maximal intensity are distanced by nearly 100 nm. At frequency 510 THz it is noticeably smaller than the half-wavelength (distance needed for the π phase shift of the plane wave in a-Si). This is a magnetic resonance because polarization currents at optically close depths flow in opposite directions. However, this magnetic mode is induced in the host material above the nanospheres. It disappears when Au nanospheres are removed. It is neither magneto-dipole Mie resonance of refractive particles [45], nor substrate-induced bianisotropy of [44], nor magnetic mode of the conventional perfect plasmonic absorber [41]. It is a specific mode of our MM layer and this mode is advantageous.

Identifying the domain of the magnetic mode as the top half of the layer

we calculated the magnetic moment of the MM unit cell using its general definition as it was done [38]. The electric dipole moment was calculated by a simple integration of polarization currents. At 500-502 THz the electric and magnetic moments are balanced and the structure represents the Huygens' metasurface. The maximal absorption (97%) is achieved at 510 THz, whereas the resonance band defined one the 70% level is nearly equal 40 THz. The reliability of our simulations is ensured by two different CST solvers – time-domain and frequency domain ones giving practically the same results (as it was in [38]).

We have also shown that the level of PV absorption and that of parasitic absorption (few percents) keeps the same in presence of the metal rear electrode on the bottom side of the structure. All the absorption practically holds namely in the PV layers (see below). Finally, the stability of the resonant PV absorption was numerically demonstrated for three incidence angles (0, 30° and 60°) and both TE and TM polarizations of the incident wave. Our PV diode implements the regime of perfect absorption without a special ARC. In our metamaterial-enhanced photodiode the resonance frequency is determined by the eigenmode and is angularly stable. Varying the incidence angle from zero to 60° we observe the shift of the resonance frequency that is nearly equal 1%. For the variant with the transparent rear electrode the resonance shifts from 510 to 515 THz. For the metal rear electrode it shifts from 526 to 533 THz.

We compared the operation of the PV diode enhanced by our nanoparticles with that of a bare PV diode (without nanoparticles). A bare diode operating in the narrow frequency band also does not need an ARC. At its Fabry-Perot resonance the reflection is damped and the absorption coefficient is rather close to unity. A bare PV diode with the same parameters as above and the metal rear electrode when it is impinged by a normally incident light has the resonance of absorption at 475 THz. At this resonance the reflection coefficient is nearly zero and the absorption coefficient equals 97%.

At a first glance, such the bare PV diode does not needed the enhancement at all. However, it is not so. First, the resonance frequency strongly depends on the incidence angle. For incidence angle 60° the resonance of absorption holds at 430 THz. Therefore, if it is impinged by a LED or a lamp radiating at frequencies 470-480 THz one needs to always adjust the position and the orientation of the microchip on which the PV diode is located. This hinders the selected biomedical application of the bare PV

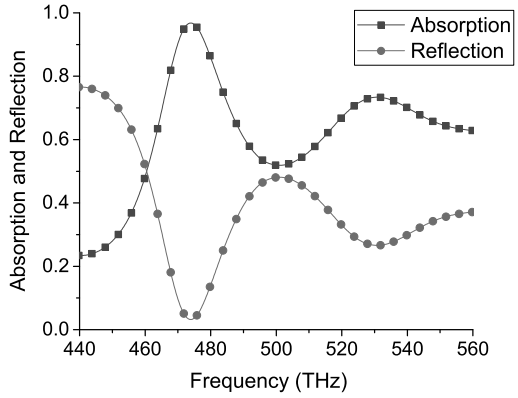

(a)

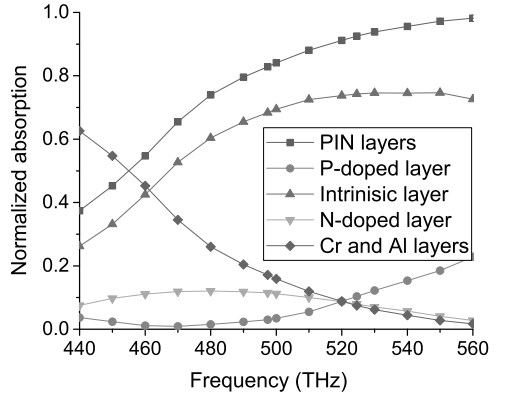

(b)

Figure 2.4. Absorption and reflection coefficients of the bare diode structure (without Ag spheres inside the intrinsic layer) for the normal incidence (a). Distribution of the absorption in all constituents of the structure (b).

diode.

Meanwhile, for the metamaterial-enhanced PV diode the frequency band of the resonant absorption practically does not change for different incidence angles. This means that the photocurrent keeps the same for different illuminations. This is the first advantage granted by our MM.

The second drawback of the bare PV diode is high parasitic absorption. In fact, almost complete absorption at 475 THz does not mean for the bare diode a real frequency maximum of the external quantum efficiency. In Fig. 2.4 we show the resonant absorption/reflection in the bare PV diode with Al substrate impinged by a normally incident wave. At the thickness resonance 475 THz the absorption in the n-doped sublayer increase and what is more important the absorption in Cr is very high because the

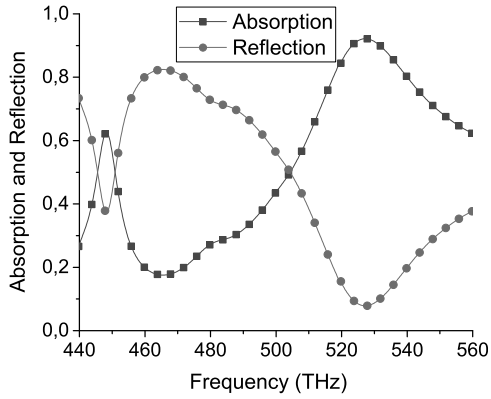

(a)

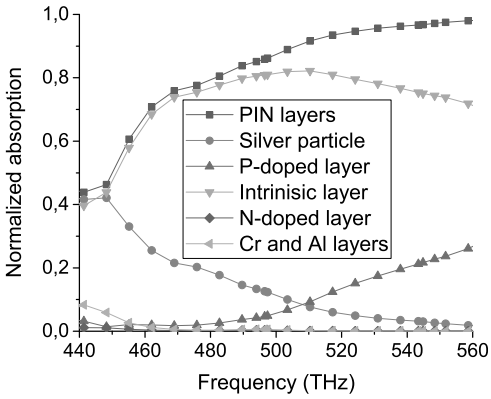

(b)

Figure 2.5. Absorption and reflection coefficients of the diode enhanced by Ag nanoparticles (a). Distribution of the absorption in all constituents of the structure (b).

maximum of the standing wave shifts downward from the central plane of the PV diode in the whole range 400-500 THz. As a result at 475 THz the total parasitic absorption (in Cr, Al and n-doped a-Si) attains 40%.

Now, let us inspect the case of the PV diode enhanced by our MM, that is depicted in Fig. 2.5. It operates at 520-550 THz, and at 526 THz the absorption coefficient attains 92%. In this band the parasitic absorption is negligibly small, if we consider the absorption in the p-doped layer as useful. The absorption in Cr and Al is absent – the wave does not attain even the n-doped layer. Therefore, the gain in the useful absorption (that in the intrinsic a-Si sublayer) compared to the bare PV diode exceeds 50% even for the normal incidence.

Besides of PV diodes enhanced by Ag nanoparticles we have also stud-

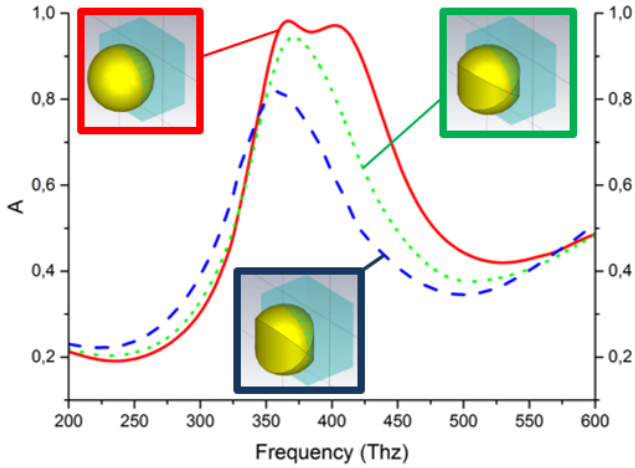

Figure 2.6. Useful absorption in the p-i-n diode enhanced by Au nanoparticles centered in the intrinsic silicon layer. The absorption frequency dependence is shown for three different levels of the particle flattening – 0, 25% and 50%.

ied the enhancement by Au nanoparticles. Silver is very vulnerable material – it oxidizes very fast and very minor quantities of sulfates spoil the nanostructures of Ag. Therefore, utilizing Ag nanoparticles for the enhancement of the PV diode one should be very careful so that not so spoil the silver during the fabrication process. From this point of view, gold nanoparticles are more practical. However, Au nanoparticles might be not exactly spherical – the deviations from sphericity up to 15-20% are possible for cheapest colloidal Au nanoparticles available on the market.

We have studied the impact of the Au nanoparticle shape flattening the spheres up to the tablets with ratio height/diameter equal to 0.5. The absorption coefficient versus frequency for the normal incidence is presented in Fig. 2.6. Here the thickness of the intrinsic layer is increased so that the Fabry-Perot resonance of the bare diode holds at 375 THz. At the same frequency the array of Au nanospheres offers the maximal absorption. The two resonances hybridize and we observe two resonant peaks – at 370 and 420 THz. In Fig. 2.6 we present the results for the case of the metal rear electrode. We see that the strong flattening of the spheres worsens the resonant absorption. Meanwhile, the ratio height/diameter equal 0.75 still keeps the resonance effect and this curve nearly reproduces that for a bare PV diode. Again, the bare structure corresponds to high parasitic losses and has no angular stability. In general, the enhancement of the angle-averaged absorption granted by gold spheres is not much lower than that offered by silver spheres. This theoretical observations was done using CST Studio software and analytical model of

the multilayer structure based on transmission matrices (see e.g. in [66]).

2.3 About practical implementation of the metamaterial photodiode

In order to get the evidence of practical feasibility of our metamaterial we have studied the impact of deviations from the optimal period. The same operation keeps for deviations within a dozen of nm. Higher deviations destroy the useful resonance. Also the distances between the Au nanoparticles should be kept optimal with the allowed deviations of few nm.

As it was noticed above such regular structures are challenging for fabrication especially on large areas. The requirement of such fabrication tolerances would cancel the usefulness of our study if among nanotechnologies there were no self-assembly. The self-assembly is one of most useful tools of nanochemistry that offers the possibility of large-area nanofabrication.

To this end, the solid Au or Ag nanospheres should be replaced by core-shell nanospheres which are also available in colloids. The Ag (or Au) core of the particle should be the same as in our simulations. The silica shell thickness is equal (in our notations) $p/2 - r_{\mathrm{Ag}}$. This shell will also protect Ag from harmful factors during the fabrication, and the use of nanoparticles with Au core is not mandatory.

First, one prepares the bottom part of the structure – that with the n-doped layer and 100 nm thick layer of intrinsic a-Si on top of it, utilizing the standard PECVD technique. On top of the intrinsic layer one creates a monolayer of mutually touching core-shell nanospheres self-assembled from the colloidal solution. How to do it using the self-assembly will be explained below. The thickness of the nanoparticle shell ensures the optimal separation of the plasmonic cores and grants the needed absorption resonance. Next, one continues the fabrication of the structure. Nanoparticles of intrinsic amorphous silicon will hopefully fill the nanogaps between the nanoparticles so that they will be incorporated into a-Si. Of course, the suggested fabrication technique needs an experimental verification. However, this experiment has not been done, yet. We hope that the claimed advantages of this design and its affordable feasibility will be experimentally confirmed in future.

3. Affordable Plasmonic LTSs for Perovskite Solar Cells.

3.0.1 Perovskite as a photovoltaic absorber

Perovskites are materials with chemical formula ABX_3 whose molecular crystal lattices can be cubic, orthorhombic or tetragonal [52]. Element A is an organic molecule called large cation ($CH_3NH_3^+$, $NH_2CH = NH_2^+$, etc.). Element B, called small cation, is a heavy metal (usually, Pb, Ge, Eu, Cu, or Sn). Element X can be I, Br, Cl or F (thus, BX_3 is a metal halide). Synthesis of PV perovskites is a cheap low-temperature chemical process [52]. Above, we have mentioned such advantages of perovskites as a remarkably high PV spectral response and high optical decay. Together, these properties result in high photocurrents achievable with a submicron layer of perovskite and imply that the optimal perovskite SC is namely a TFSC.

Historically, perovskites were for the first time used in solar photovoltaics as nanoparticle counterparts of the dye molecules in so-called dye-sensitized solar cells [53]. This resulted in the record (for that time) of the power-conversion efficiency for dye-sensitized solar cells. After, extensive studies the physics of this effect – PV conversion in perovskite itself – was established. The internal quantum efficiency of PV perovskites strongly exceeds that of all other known materials of TFSC. It is twice higher than that of a-Si and is nearly equal to that of c-Si, GaAs or Ge. Since the publication of [53] the overall conversion efficiency of perovskite-based solar cells has grown by an order of magnitude. Nowadays, the record efficiency for perovskite SCs (very thin and extremely cheap) exceeds that of amorphous silicon SCs [54]. Even flexible perovskite SCs are 1.5 times more efficient than the hard TFSCs based on a-Si with the polished metal electrode. This progress allowed many researchers to claim a new era in solar photovoltaics [55]. The main issue, as it was mentioned above, the stabil-

ity of operation. In this field the progress is also significant – the lifetime of materials used in perovskite SCs has increased since 2011 from few hours to hundreds of hours. But it is still not sufficient for commercialization of perovskite SCs. Anyway, we do not doubt that the lifetime of perovskite SCs will exceed a year in the nearest future.

We have already mentioned that perovskites are exitonic PV materials like dyes or arrays of quantum dots used in organic SCs. However, unlike them they also possess a rather noticeable conductance for electrons and holes [54–57]. This allows one to perform a heterojunction of a perovskite with electron-conductive and hole-conductive materials like the heterojunction in the p-i-n diode. The role of intrinsic a-Si is played by the perovskite layer, whereas the electron-conductive layer plays the role of n-doped a-Si and the hole-conductive layer plays the role of p-doped a-Si. A high-efficient perovskite-based solar cell is TFSC. For the perovskite layer of thickness 500 nm the transmission losses in the bottom electrode are negligible [54, 55, 57].

The optimal thickness of the perovskite layer is determined by the deal between two parasitic effects. First, one has to minimize parasitic shunts formed by the amorphous materials – electron-conductive and hole-conductive ones. They meet one another due to the diffusion in the nanopores of perovskite. This effect requires to increase the thickness[1]. Second, one has to decrease the recombination losses drastically growing versus the thickness of the PV layer when it exceeds the exciton size. Also, the Ohmic losses in the perovskite layer grow with its thickness. As a result, the optimal thickness of pervoskite is defined as 400 nm, that corresponding to nearly 10% for transmission losses. Thickness 500 nm for which the transmission losses completely disappear is still close to the optimal one, and there is no noticeable difference in the overall efficiency for perovskite SCs with 400 nm and with 500 nm perovskite layers. Both electron-conductive and hole-conductive layers forming the Ohmic contact with perovskite are, as a rule, thinner. The n-conductive layer on top is as thin as 40-50 nm, that allows to neglect the optical losses in it. The p-conductive layer may have the thickness 200-300 nm. As a result the PV structure of a typical pervoskite SC has the overall thickness 600-800 nm [57]. The top electrode is performed of TCO, and the bottom is, as a rule, a layer of metal.

[1]Not only this effect – also parasitic capacitance of the PV diode, parasitic hysteresis and transmission losses reduce when one increases the perovskite thickness.

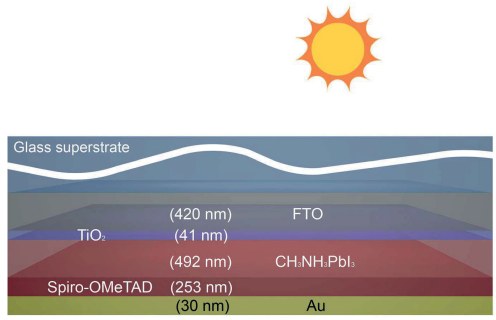

Figure 3.1. Schematics of the practical heterojunction configuration of a high-efficiency perovskite-based solar cell in accordance to [63]. The anti-reflecting coating on top of the superstrate is not shown.

It is commonly adopted that perovskite TFSCs with thickness of perovskite 400-500 nm do not need a LTS. It is enough to suppress the reflection in order to achieve the maximal optical efficiency. This s done adjusting the thickness of the transparent electrode. The use of titanium dioxide as the n-conducting material allows one to utilize the fluorine-doped tin oxide (FTO) as the material of this electrode as forming the Ohmic contact with TiO_2. This material has lowest refractive index among TCOs (1.5 in the visible range and 1.4 in the near IR), that allows its application also as an ARC. Optical losses in this material are as low as in AZO. Therefore, the laminate of such TFSCs is not a polymer but glass, perhaps, organic glass (PMMA).

The optical efficiency of such a SC is restricted only by nonzero reflection losses (near 15%) inevitable in the case of the wide-angle operation and attenuation of the incident light in the FTO electrode that nearly equals to 10% for the structure depicted in Fig. 3.1. Integral angle-averaged optical efficiency 75% and integral Ohmic loss 5% correspond to 15% for the overall efficiency of this SC [56, 57].

3.1 Perovskite thin-film solar cells enhanced by metallic particles

However, perovskite SC may need a LTS, if the bandgap wavelength is larger than 870 nm. Optical losses 25% calculated in [56] and [64] for the structure sketched in Fig. 3.1 do not take into account the sub-bandgap losses. They were calculated for the case when the perovskite bandgap wavelength is equal 800 nm, and the IR tail of the solar spectrum was ignored.

Perovskite $CH_3NH_3^+PbI_3$ is a bandgap-tunable material and its bandgap

can be engineered in the range of wavelengths 700-1000 nm [65]. When the bandgap is above 870 nm the solar radiation around the 870 local peak of the solar spectrum will be also converted. However, all PV perovskites have low absorption in this range with the local minimum namely at 870 nm. Then transmission losses arise at this wavelength even for perovskite as thick as 492 nm, as in Fig. 3.1.

Consider the SC depicted in Fig. 3.1 abstaining of the reflection losses (e.g. assuming that on top of the laminate of organic glass there is an ideal anti-reflecting coating). Then the incident wave can be assumed to be incident from the half-space of glass to the top interface of the structure (glass-FTO). For our purposes, it is enough to consider the normal incidence of the solar light. The dimensions of the simulated structure are depicted in Fig. 3.1 and correspond to the practical solar cell [56, 63, 64]. The FTO layer is 420 nm thick, 41 nm is the thickness of TiO_2, 492 nm is the thickness of the $CH_3NH_3^+PbI_3$ perovskite, and the hole-conducting layer (the so-called spiro-OMeTAD) is 253 nm thick. The gold rear contact has the thickness 30 nm. A so small thickness of the bottom electrode was chosen for the reduction of the price per square meter (the further reduction will increase the Ohmic losses in this electrode). The properties of the mechanic carrier beneath the gold do not play any role, since the incident wave does not transmit through the structure.

We have calculated the absorption in each of these layers using both CST Studio software and analytical model of the multilayer structure based on transmission matrices (see e.g. in [66]). Material parameters of all these layers have been taken from [63]. The results of these simulations coincided with high accuracy and visually are not distinguished in the plots. In Fig. 3.2 we show the simulated coefficient of the photovoltaic absorption (percentage of the incident power spectrum absorbed in the perovskite layer) over the whole solar spectrum. We can see two significant dips of absorption centered at 870 and 1000 nm. In the inset Fig. 3.2(a) we show the spectrum of radiation absorbed in the perovskite. In these calculations the solar irradiance spectrum (shown as a in shadow this inset) was multiplied by the absorption coefficient of the layer calculated using the analytical model. This spectrum implies that 3% of the solar radiation transmitted to the perovskite is lost due to parasitic transmittance. Nearly 2% of the incident solar power is lost in the range 820-940 nm and 1% – in the range 970-1050 nm.

Using a plasmonic LTS incorporated into perovskite it is possible to

avoid the 2% loss at 820-940 nm. The presence of the plasmonic MM increases the absorption in the perovskite around the nanoparticles within the spectral hole of the perovskite absorption 870-950 nm. The increase is nearly 30% and is not accompanied by the distortion of the photovoltaic absorption at other wavelengths. We engineer resonant absorption at 870 nm. The same regime as in the previous Chapter is utilized – the absorption in Au is negligibly small, and all the increase of the absorption is useful.

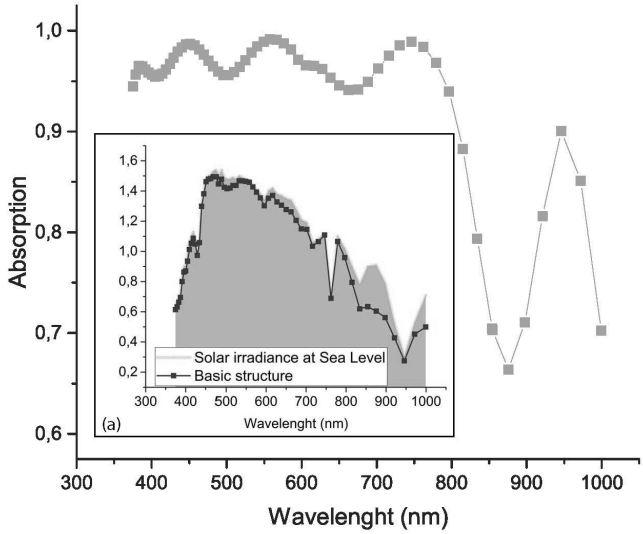

Figure 3.2. Absorption coefficient of the perovskite layer in the structure shown in Fig. 3.1 versus wavelength. In the inset (a) we show the solar spectrum AM 1.0 in arbitrary units (shadowed) and the spectrum of absorption in the perovskite layer.

Of course, in order to justify a so small gain in the optical efficiency as 2% the fabrication cost of our plasmonic array has to be low. We hope that it will be low if we use the femtosecond-laser-induced forward transfer technique – LIFT technique [67, 68] in order to incorporate the gold nanoparticles into perovskite. In the previous chapter we suggested to fabricate the PV layer in three steps – first, the bottom part, then the array of nanoparticles, on top of it, and then the top part. This procedure is time consuming. Perovskite is softer than a-Si and is porous that allows to use a so fast fabrication technique as LIFT. LIFT is a high-speed and low-cost technology which simultaneously produces metal or even dielectric [69, 70] nanoparticles and transfers them to the target host. The host should be either soft like polymers or porous like perovskites. The

laser locally melting the golden film is assumed in this picture moving from the right to the left. Both averaged inter-particle distance and particle size can be independently controlled by laser focusing conditions and the energy in the laser pulse. The depth of the embedding into the target substrate depends on the distance to it from the Au film serving the source of nanoparticles . It is worth noticing that both the temperature and velocity of the embedded nanoparticle are also controllable [69], making possible the transfer of either hot or cold nanoparticles. In our case LIFT is especially suitable as the studied effect does not require strong periodicity.

The perovskite SC shown in Fig. 3.1 can be produced from top to bottom, i.e. prepared on the glass substrate (which can be later reduced to the optimal thickness and furnished by the anti-reflecting coating). Therefore, before covering the perovskite with the Spiro-OMeTAD one may put on the perovskite a glass plate covered by a gold film with 240 nm thickness and to apply the LIFT technique. The gold film transforms into Au nanoparticles of diameter 240 nm submerging into perovskite. Next, the glass plate is removed and the fabrication continues.

Notice, that, to our opinion, LIFT is a promising candidate to fabricate plasmon-enhanced solar cells of 3d generation – besides of pervoskite solar cells there are several solar cells in which irregular arrays of plasmonic particles may enhance the overall efficiency due to different physical mechanisms [79–81].

Fig. 3.3 shows the absorption spectrum in the perovskite layer calculated using CST software. This spectrum is determined by the solar irradiance whose spectrum is shown again as a shadow and absorption in the perovskite surrounding the incorporated plasmonic nanoparticles. In this design that are not centered in the PV layer but are located on the interface of spiro-OMeTAD. The area under the absorption curve normalized to the area under the curve of the solar irradiance is the absorption efficiency. This value for the basic structure is nearly equal 92% (5% of power is lost in FTO). We show our results for two types of golden nanoparticles – solid Au nanopsheres and golden nanoshells (core-shell particles with the same overall radius 120 nm and a gold shell thickness 30 nm). Notice, that we have studied the impact of the particle size and period. The effect keeps for deviations $\pm 10\%$. Also, the structuring of the nanoparticle does not give a qualitative effect. For the structure enhanced by solid nanospheres the absorption of the solar irradiance in the perovskite layer

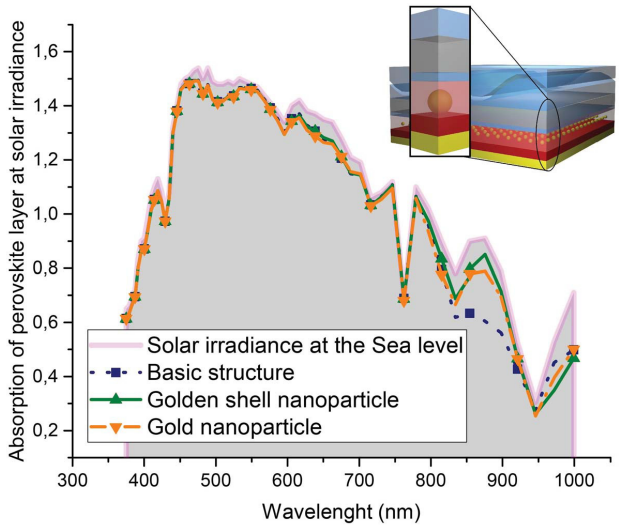

Figure 3.3. Absorption in the perovskite layer for several variants of our solar cell (basic structure, the structure enhanced by solid nanospheres, and that dielectric nanoparticles enhanced by a gold nanoshell) taking into account the solar irradiance spectrum.

is equal 93.2%, and for nanoshells it is 93.8%.

In this Chapter we have shown for the first time that the plasmon resonances of an array of Au nanoparticles may enhance the perovskite SC. Though the enhancement is small, the effect is qualitatively new. If we extend our structure beyond solar photovoltiacs, its practical importance may be much higher than it seems now. Perovskite PV cells may operate not only as SCs. Tunability of the bandgap may allow them operate as narrow-band PV diodes even at infrared. The narrow-band operation may be granted by an optical filter located on top of the structure instead of the glass laminate shown in Fig. 3.1. For such the PV diode operating at 820-940 nm the transmission losses are as high as 30%. As we have already noticed, in the range 820-940 nm the PV absorption due to our array increases nearly by 30%. Our nanoparticles eliminate the transmission losses in this band almost completely.

In the end of this chapter it is important to notice that, in fact, gold nanoparticles without silica encapsulation cannot be used for the enhancement of perovskite SCs. As it was shown in [91] (this work was published after the submission of our paper), gold nanoparticles spoil the perovskite layer due to the atomic diffusion. Therefore, only core-shell particles (that promise the best enhancement) can be incorporated into the perovskite layer. This is also possible using the LIFT technique, however, requires a more elaborated procedure.

4. Ultra-broadband wide-angle light-trapping by micron-sized spheres.

4.1 Colloidal nanoparticles for enhancement of thin-film solar cells based on amorphous silicon

4.1.1 Technical solution and its physical prerequisites

When we suggest to improve a TFSC using a nanostructured ARC or LTS, we must take into account not only the efficiency but also the possible cost and the compatibility of the design with the mass production, especially roll-to-roll technological approach. From this point of view, an ARC of colloidal silica nanoparticles is very advantageous. Recall , that for a-Si TFSCs with a top electrode performed of a conductive material this ARC exhibits the wide-angle antireflective operation. The affordable location of this ARC on the surface of TCO is achieved via the self-assembly and fixation of the colloidal silica particles by the polymer laminate covering the TCO. The self-assembly into a monolayer of dielectric nanospheres from the colloidal solution is usually lounged by spin-coating [31,32]. However, even this process can be simplified – the self-assembly of nanospheres on a non-metal substrate can be achieved by a straight mechanical movement of the sample though a colloidal solution. The key point of such self-assembly is the properly chosen speed [34,35].

In absence of the defects this densely packed monolayer ARC has nearly the same operational characteristsics as a flat nanolayer of effective medium with refractive index close to 1.4. However, this ARC is cheaper since no nanometer precision is required to respect during its fabrication. Moreover, due to wide-angle operation, this composite ARC has lower angle-averaged reflection losses [34]. For a TCO whose typical refractive index is close to 2, the diameter of silica spheres in the ARC is equal 500 nm [8].

However, we have already seen that due to high transmission losses even an ideal ARC gives a very minor improvement of the optical efficiency of a-Si TFSCs with the PV layer as thin as 300-400 nm. For such TFSCs we need to replace the ARC by a LTS. Our idea is to modify the ARC of silica spheres increasing the diameter of spheres so that they could focus the sunlight into the PV layer and anyway would keep the antireflective functionality.

Here, we have to make an important remark. In the abundant literature of LTSs for a-Si TFSCs it is claimed that the light trapping for preventing the parasitic transmission in a-Si SCs with the flexible bottom electrode must be a subwavelength effect. The needed concentration of light is, in accordance to the literature, not achievable via the simple focusing. This is the prerequisite from which the whole plasmonic light-trapping for TFSCs arose as a scientific direction [71–75]. Above, we developed the plasmonic LTSs for narrowband light-trapping where this approach is reasonable. However, we need now a broadband light-trapping. Here I reject the plasmonic way to the target. Recall, that we found an affordable approach to the fabrication only for spherical plasmonic particles. For regular arrays of complex-shape metal nanoparticles the multi-resonant enhancement of the PV absorption is achievable but the fabrication of such arrays is expensive. For random arrays of metal particles the overall enhancement of the PV absorption is either absent or compromised by the losses in the metal.

Therefore, we have decided to revise the prerequisite of the plasmonic light-trapping for TFSCs. And we saw that the whole paradigm of light-trapping for a-Si TFSCs is incorrect. A simple diffraction-limited focusing by a usual lens is sufficient for concentration of sunlight in a layer of a-Si with thickness 300-400 nm. Really, a-Si has the refractive index close to 4 in the operation band λ =400-800 nm. In this band the effective wavelength in the material (and, therefore, the Rayleigh size of the focal spot) is as small as 100–200 nm. But 200 nm is smaller than the optimal thickness 300 nm. Next, a short-focus lens may have a focal spot at a similar distance as the spot size. Therefore, a simple short-focus lensing is all we need for light-trapping in a-Si TFSCs.

However, if we put a macroscopic short-focus lens on top of a TFSC it will collect the sunlight from the large area into one submicron-sized focal spot. The other volume of the PV material will remain dark and the photocurrent will be generated only in a submicron part of the SC. To ex-

cite the photocurrent in the whole TFSC we need an array of microlenses covering the whole surface of our TFSC. Then we immediately come to the idea of colloidal silica spheres similar to those used for ARC. Silica spheres are available on the market with diameters from 100 nm to few microns. It remains only to find a suitable diameter of the sphere and book the needed colloidal solution. The optimal diameter is found from the following deal.

When the diameter of a sphere grows the period of the densely packed array increases, too. As it is commonly known from the theory of diffraction grids, when the array period exceeds the wavelength, the Fraunhofer diffraction lobes arise in the reflected (more exactly – backscattered) field. These diffraction lobes are comparatively small if the diffraction grid is performed of a transparent material, but the amplitudes of the Fraunhofer maxima increase versus the grid period. Numerical studies have shown – backscattering losses becomes critical and the anti-reflective action of the monolayer disappears when the diameter of spheres exceeds 1.5-2 micron.

From the theory of a spherical microlens, it is known that it operates with visible light like a macroscopic spherical lens if its diameter exceeds 5-10 microns [76]. However, to replace 500 nm-large spheres used in the ARC by 5 micron-large spheres operating as microlenses is not a proper solution. Of course, an array of microlenses will prevent the transmission losses. However, backscattering losses will be too high in this case and there is no enhancement.

Fortunately, for 1-1.5 micron-large spheres the optical effect resulting in the light concentration has been recently revealed in work [77]. It is called photonic nanojet. Its theory was developed in [78]. This effect is formation of a collimated light beam by a microsphere impinged by a plane wave. This is not the resonance effect but it is sensitive to the wavelength. Physically, the collimation of the wave beam results from interference of spherical harmonics produced by a uniformly illuminated dielectric sphere in the forward-scattered field. The light beam resulting from this effect is collimated if the sphere size exceeds at least twice the effective wavelength in the material of which the sphere is performed. When the sphere diameter becomes optically large this collimation is smoothly substituted by a usual focusing [78]. For a 1 micron sphere the light nanojet is formed in the whole visible range [78]. And 1 micron period for such an array still corresponds to sufficiently low reflection losses. This is how

we found the optimal diameter of the spheres.

So, a monolayer of densely packed silica micron-sized spheres operates as a homogeneous wide-angle ARC for the reflected sunlight and as an array of light-collimating lenses for the sunlight transmitted into the PV layer. A so unusual combination of optical properties allows us to refer such the LTS as MMs, though the constituents of this array are not resonant in the band of our interest.

4.2 Theoretical analysis of enhancement granted by our metamaterial: comparison with anti-reflecting coating

During theoretical analysis the optimization of design parameters was done for all possible angles of incidence taking into account the path of the Sun for the explicit geographic altitude and the typical tilt of the roof on which the TFSC panel usually mounted. Therefore we simplified our task for numerical simulations of daytime-averaged optical efficiency restricting it by three incidence angles - 0, 30°, and 60°. Our optimum refers to the arithmetic mean value of the photocurrent simulated or measured for these three angles[1]. To our estimations, such a simple approach is relevant for a solar panel located under the altitude of Helsinki on the southern side a flat roof with typical tilts 20-30° with respect to the horizontal plane.

In our simulations we compared our LTS with a flat ARC. For a flat ARC we used a standard Matlab code based on transfer matrices. These calculations are very fast and allowed us to study all angles of incidence from 0 to 75° (edges of the daytime). The best daytime-averaged operation of the flat ARC is achieved when the thickness of silica (80 nm) is chosen so that to maximally suppress the reflection at 30°. Our numerical analysis has shown that for the this angle and even for the normal incidence our LTS of silica spheres is not advantageous compared to the ARC. It gives an increase of the PV absorption compared to the bare SC but the ARC operates better.

In order to explain it, we have to notice that even a bare TFSC has a sufficiently small reflectance over the whole visible range where the TFSC operates. Our bare TFSC is optically a multilayer structure, and it is possible to adjust its layers in order to minimize the normal-incidence

[1]Applications of the dielectric spheres on top of the SC can change neither the fill-factor nor the open-circuit voltage of the SC. Therefore, the gain in the efficiency equals to the gain in the photocurrent.

reflection in a broad range. Both front and rear electrodes are performed of AZO and the substrate of our TFSC is glass wafer. An especially important factor is the thickness of the top electrode. Its proper choice (220 nm) allowed us to reduce the reflection losses for the normal incidence to 9% and the angle-averaged value of the reflection losses is nearly equal 20%. The application of 80 nm of silica on top additionally reduces the spectrum-integral power reflectance – for the normal incidence to nearly 2% and the day-time averaged reflectance reduces to nearly 13%. It is a very low reflection loss for the wide-angle regime that it is difficult to improve once more. In our simulations, our LTS operated similarly and all the gain granted by our LTS refers to the elimination of transmission losses.

Of course, a flat ARC cannot prevent the transmission losses, whereas our LTS suppresses them very well. However, for small angles of incidence the suppression of the transmission losses is not sufficient to increase the photocurrent. The increase of the photocurrent is not simply proportional to the PV absorption because the light collimation by nanospheres for the small incidence angles is individual for every sphere. The photocurrent density achieves the saturation at the collimated beam centers when all the flux is absorbed and vanishes beyond the collimated beam where the flux is zero. As a result, the photocurrent per unit area of our TFSC for $\theta = 0$ and $\theta = 30^\circ$ increases compared to the bare SC only slightly.

For large angles of incidence the situation drastically changes. A new optical effect we called the cascade collimation is now involved. Namely, only a part of the wave beam incident on a given sphere under sufficiently large angle (practically more than 40°) is collimated in the air gap formed by the adjacent spheres and its refraction into the PV layer creates a collimated beam under the point where two spheres touch one another. Another part of the incident beam (nearly 50% of the power) transmits to the adjacent sphere as it is shown in Fig. 4.1. In this second sphere the wave beam experiences three total internal reflections and the collimated beam arises under the center of the second sphere. In fact, this simplified picture corresponds to the cylindrical geometry. For spheres the oblique incidence on one sphere corresponds to the formation of four collimated beams. As a result, these multiple collimated beams fill the area beneath the spheres.

This consideration based on the geometrical optics is, of course, simplistic. However, the key point – four-fold multiplication of light nanojets for

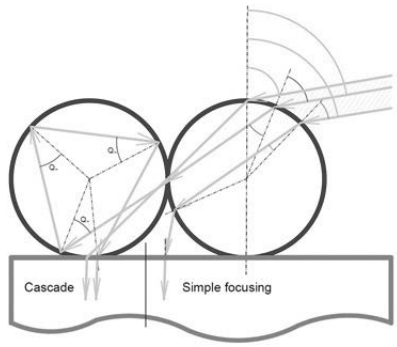

Figure 4.1. Schematic view of mechanism of cascade focusing.

$\theta = 60°$ – keeps in our simulations. And the photocurrent density distribution over the horizontal plane becomes almost uniform.

Simulations (we have done using different solvers) have shown – if we optimize this LTS for the whole range of incidence angles corresponding to the daytime we achieve an advantageous operation compared to the similarly optimized ARC. The results of simulations for the expected gain in the ultimate efficiency of the PV conversion compared to the bare TFSC granted by either ARC or our LTS for different incidence angles are presented in the table.

Table 4.1. Gain in the overall efficiency η.

Gain % / $\theta°$	0	30	60
ARC	+8	+36	-1
LTS	+15	+16	+70

Exact parameters of the simulated TFSC are (from down to top) as follows: the rear AZO layer of 270 nm, the n-doped a-Si (with density of majority carriers 10^{20} 1/cm^3) of 70 nm, the intrinsic layer of 400 nm, the p-doped a-Si of 100 nm (density of majority carriers 10^{18} 1/cm^3), and the front AZO layer 220 nm. ARC was 80 nm-thick of silica. Spheres of silica with 1 micron diameter form a densely packaged monolayer. In accordance to Table 4.1 the mean gain granted by our LTS compared to the bare SC is equal 34%, and that granted by the ARC is 9%. Our LTS improves the overall efficiency compared to the ARC by 17%. This corresponds to practically complete removal of transmission losses.

4.3 Experiment

4.3.1 Discussion of the cell geometry

Here we present the results for the a-Si TFSC with 400 nm of intrinsic silicon. We have to explain this our choice, since the optimum is 300 nm, and most of papers on LTSs for a-Si TFSCs refer either to the design solution with either this optimal thickness or thinner. However, 400 nm is better for our purposes. It is not much thicker than the optimum and still corresponds to rather low recombination losses. What is important for us, is to prevent the interplay of reflection and transmission losses. Our TFSC has minimal possible transmission losses that allows us to concentrate on the impact of transmission losses. The structure with a so substantial intrinsic layer turned out to be less reflective. The second reason why we selected 400 nm is its easier implementation. The design with a 300 nm thick intrinsic layer would require 30-50 nm thick layers of doped a-Si and much higher doping level, not achievable for us.

Notice, that the use of 400 nm layer of intrinsic silicon advantageously shares our work from the row of similar studies. So substantial PV layers in the literature on LTSs, to our knowledge, are absent. We think that the reason of it is the difficulty to demonstrate an advantage of any of previously known LTSs compared to an ARC for a so substantial PV layer.

Notice, that we have simulated TFSCs with several thicknesses of the PV layer, not only 400 nm. In our simulations the advantage of our LTS compared to an ARC was obtained for design solutions with a PV layer whose thickness exceeds 300 nm. For thinner PV layers our mechanism of the light concentration (light collimation) is not efficient. However, 400 nm is not an optimum in our calculations. In accordance to our simulations, the gain granted by our LTS compared to the ARC is maximal for the thicknesses of the intrinsic layer within the range 300-350 nm, when the p- and n-doped layers are 50 nm thick. However, it is important that the advantage of our LTS with respect to the ARC still keeps for the design with a 400 nm thick intrinsic layer, that corresponds to the minimal reflection losses and that is easier to fabricate.

For the experimental check we have chosen this variant and this is why in Table 4.1 we show the results namely for it.

4.3.2 Fabrication

A set of samples with in-plane dimensions 1×2 cm was fabricated in the clean room of Micronova Center of Aalto University. Since our facilities are not appropriate for preparation of TFSCs, we have developed an original method. First, we cover the glass wafer with AZO using the ALD process [35]. The mean value (averaged over the samples) of the thickness of this rear AZO layer is 272 nm. Next, we cover our samples with a 570 nm (mean value) thick p-i-n structure of a-Si using the PECVD and the standard ion implantation.

For it, we, first, deposit the 70 nm thick layer of intrinsic a-Si on top of the AZO layer using PECVD. Next, we dope this layer with Boron beam of energy 20 keV using Ion Implanter Eaton machine until the majority carrier concentration $10^{20}cm^{-3}$. It is insufficient doping for obtaining maximal fill-factor and corresponds to decreased open-circuit voltage. For optimal operation the concentration of the bottom doped layer should be higher by 3 orders of magnitude [33]. But our equipment is dedicated to crystalline silicon SCs and does not allow us to achieve higher concentrations in the p-doped layer. Also, usually, a p-doped layer is built on top of the SC because it is more transparent for the same doping level than the n-doped one. However, I have inverted this typical scheme so that to avoid the parasitic p-n junction. The reason is that typically one uses AZO only in the cathode, but we use AZO as a material for both anode and cathode[2]. AZO has the p-type conductivity, and the anode of AZO forms a p-n junction with the n-layer of the usual p-i-n structure.

Then we deposit by PECVD a 500 nm thick layer of intrinsic amorphous silicon and dope top 100 nm of this layer by Ion Implanter Eaton with energy 10keV (phosphorus gas) until the concentration of majority carriers $10^{18}cm^{-3}$. For this concentration the optical losses in the n-doped layer do not noticeably exceed those of the intrinsic layer. Also, the PV spectral response of this slightly doped layer is higher than that of the heavily doped. Therefore, the effective PV layer in this case has the thickness practically equal to 500 nm. On top of this p-i-n structure we deposit a layer of AZO of thickness 221 nm (mean value). It is done using ALD.

My structure has not very high quantum efficiency, but this efficiency is not the target. The main purpose is to reduce the reflection losses as much as possible and to concentrate to the transmission losses. First, I

[2]In order to minimize the reflection losses, as it was explained above.

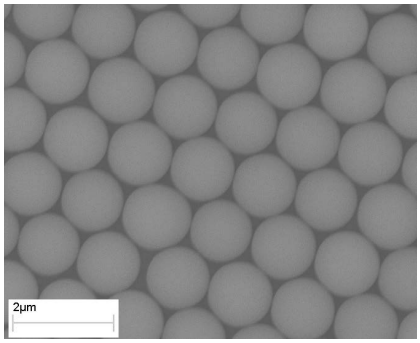

Figure 4.2. The quality of our LTS within the area of mutually touching spheres is illustrated by the SEM image.

prove that transmission losses are high even for a substantial PV layer. Second, I prove that developed LTS grants the enhancement namely due to the suppression of transmission losses.

One third of all fabricated samples of our TFSC was left bare. Another one third was covered with a 85 nm thick (mean value) layer of silica using the PECVD[3]. The other samples were covered by silica spheres with $d = 1.0 \ldots 1.2\,\mu$m. This deviation of diameters is typical for available colloids. We utilized the method of natural deposition (self-adhesion) of nanospheres suggested and developed in works [31] and [34]. It was already mentioned that this method results in a densely packed monolayer on the mm-sized areas. These good areas formed mm-sized islands on our cm sized samples. In between these islands the areas (also mm-sized) of isolated spheres and bare areas are located. The high-quality area is shown in Fig. 4.2. In our measurements we illuminated only these high-quality areas of the sample using the light-concentration technique with a collimated beam of simulated sunlight with one mm cross section. The beam was tilted under the angle θ varying from zero to $\theta = 60°$. Practically, we compared mm sized TFSCs covered with spheres with mm sized TFSCs covered with an ARC and with mm sized bare TFSCs. The results of the numerous measurements were averaged.

4.3.3 Measurements

The measurements of the reflection (backscattering) losses with an integration sphere for three incidence angles has shown that our ARC grants nearly 30% of reduction for the angle-averaged integral reflectance com-

[3]The measurements using the Profilometer Dektak/XT have shown that the thickness of silica in ARC is within the interval $h = 80-90$ nm. The relative deviation $\pm 5\%$ is typical for all layers of our structure obtained by PECVD, whereas ALD gives the deviation smaller than 2 nm, the same refers to the roughness.

pared to the bare SC, namely this reflectance reduces from 21% to 14%. This experimental result is in agreement with calculations reported above. We have also confirmed that the gain granted by our ARC is maximal for the angle $\theta = 30^{\circ}$, and in the experiment it nearly equals 25 %.

We could not measure separately the spectrum of the PV absorbance $A(\lambda)$ that cannot be separated from the parasitic absorption in AZO and in the doped a-Si. However, we can judge on the PV absorption based on the measured external quantum efficiency (QE) of our TFSC. These spectral measurements were done using the Solar Spectral Response/QE/IPCE Measurement System delivered by PV Measurements, Inc. Theoretically, QE is proportional to $A(\lambda)$ and these experiments have shown the very good correspondence of the measured spectrum with the simulations of the PV absorption. The low maximal value of QE is related with the insufficient doping level of a-Si as discussed above. Again, my goal is not to fabricate an excellent SC but to prove the higher efficiency of the LTS in comparison with the ARC. And this comparison is convincing if the thickness of the PV layer is not intentionally reduced compared to the optimum (300 nm) in order to stress the advantage of the LTS. In my study I, on the contrary, enlarged this thickness, and still obtained the gain due to our LTS.

Illuminating our mm-sized TFSCs by a collimated sunlight I have seen that in the samples covered by silica spheres only the high-quality areas to operate properly. Corresponding results for the external quantum efficiency and photocurrent were taken into account. The worst results corresponded to the illumination of the bounds between the good areas and defect areas with isolated spheres. High scattering losses correspond also to the illumination of defect areas. Meanwhile, in these samples there were also bare areas without spheres, The illumination of these areas gave basically the same results as the illumination of bare cells. Since the measurements in the integration sphere do not allow one to use the narrow collimated beam, we could not measure the backscattering losses for samples covered with microspheres. However, all other results of the measurements are in very good agreement with the theory. And this theory predicts the same antireflective operation of the LTS.

The experimental result for external QE statistically averaged over the samples of three types is shown in Fig. 4.3. In this figure EQE is limited between 500 nm and 700 nm due to the low quality of manufactured experimental PV devices. The deviations of the results obtained for different

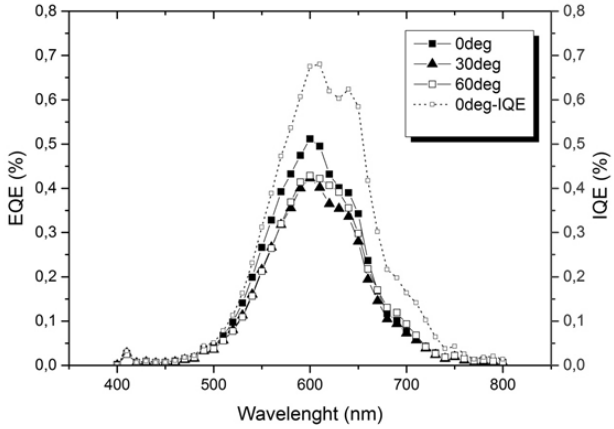

Figure 4.3. Measured external quantum efficiency of the plain TFSC for different angles of incidence θ and internal quantum efficiency for normal incidence.

TFSCs of the same type were much smaller than the difference between the mean results obtained for the three types of TFSCs. In agreement with the theory the largest gain is achieved for $\theta = 60^\circ$ and the spectral curves for QE almost repeat the theoretical curves for the absorbance. This agreement refers to all types of TFSCs under comparison – bare TFSC, that with ARC and that with LTS.

Finally, I have measured the photocurrent J induced in all samples using the same collimated beam tilted with different angles. In the case of TFSCs enhanced by the LTS I illuminated only the areas covered by a proper LTS. The current J was measured with the digital multimeter Keithley-196. The measurement code was written in the NI Lab View shell. The gain in J is practically equal to the integral gain in QE because the open circuit voltage and fill factor do not depend on the presence or absence of ARC and LTS on top of the structure. The results for the gain granted to the TFSC by both ARC and LTS are presented in 4.2.

Table 4.2. Gain in the photocurrent J.

Gain % / θ°	0	30	60
ARC	+14	+25	+10
LTS	+9	+17	+71

The mean gain due to ARC is equal 16%, whereas that offered by my LTS is 32%. The agreement of the experiment with the theory above is excellent.

4.4 Conclusions for ultra-broadband wide-angle light-trapping by micron-sized spheres.

I got numerical and experimental evidences that the properly designed LTS performed as a densely packed array of silica microspheres applied on top of a a-Si TFSC is noticeably more efficient than the ARC. This is so because the LTS combines two functionalities – preventing the parasitic transmission and damping the reflection. I have designed presented structure so that the antireflective action of the LTS is the same as that of the ARC, and the whole gain granted by the LTS refers namely to the elimination of transmission losses.

To our knowledge, my work [82] was first to experimentally demonstrate a nonzero angle-averaged gain in the efficiency granted by a light-trapping structure compared to anti-reflective coating for a solar cell based on the amorphous silicon with the intrinsic a-Si layer thicker than 200 nm.

5. Ultra-broadband wide angle light-trapping structures implemented in the top electode

5.1 From spheres to hemispheres

After my work [82] it has been clear that the suggested method of fabrication does not allow us to prepare the LTS on large areas without defective regions. Since in practical applications TFSCs are impinged by natural sunlight that is not focused or collimated, we should have eliminated these defective domains. Cleansing these areas or cutting them off is hardly attractive for industrial adaptation of these SCs. We needed to design another LTS still affordable, still broadband, still efficient but either free of fabrication defects or not so sensitive to the quality of fabrication.

I managed to resolve the problem of the second way – I have found a structure whose defects do not scatter as much as the defects of our previous LTS. Recall that these defects are isolated dielectric spheres and small (few microns) clusters of spheres on top of a flat substrate. They create a very strong scattering. What about hemispheres? Perhaps they are not so strongly scattering, and perhaps they are still capable to create photonic nanojets.

I have started from answering the second question. Unit cells of the three arrays under study are depicted in Fig. 5.1. I have found the range of values for the radius r that corresponds to the formation of the photonic nanojet in the visible range. On the right panels of all sketches I depict typical color maps of the photonic nanojet in the substrate structured in accordance with the geometry of SC. In these simulations the light at wavelength 600 nm was incident normally. For all three structures the effect is broadband – the similarly collimated beams are formed at other wavelengths – in the band covering the most part of the visible range.

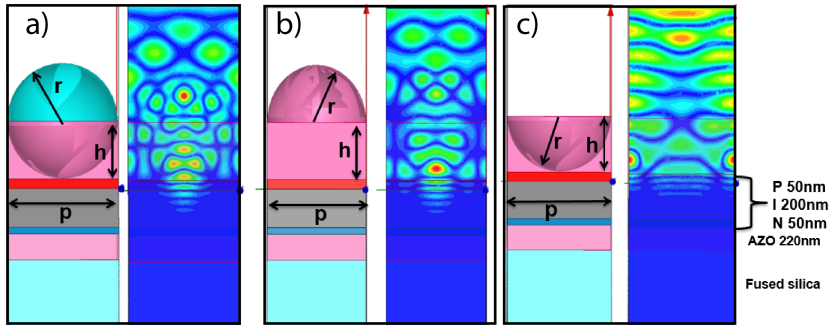

Figure 5.1. Three micron-sized objects may concentrate the light in the PV layer of a-Si: a) a spherical inclusions of silica submerged by one half into the top electrode, b) a hemispherical boss on the top electrode performed of the same material, and c) a hemispherical dent in the top electrode. On the right panels one may see typical color maps of the photonic nanojet in the substrate structured in accordance with the geometry of a typical TFSC. Design parameters of the TFSC are also shown.

For the formation of the nanojet it is required that the thickness of the top electrode (AZO) h is equal or larger the radius r. In all three cases depicted in Fig. 5.1 $h = r$.

I have numerically simulated the PV absorption in a TFSC (its geometric parameters are shown in Fig. 5.1) granted by three types of LTSs formed by densely packed arrays of these objects located in the top electrode of AZO. In Table 5.1 I compare these three structures via the integral difference of the PV absorption. In the same table, I also show the results for our previous LTS and for a flat ARC. Here, the PV absorption for a bare TFSC is taken as a reference. The values of r were optimized (varying with the step 50 nm) for all three new LTSs. For the case illustrated by Fig. 5.1(a) we have $r = 550$ nm for the optimal radius, for the structure shown in Fig. 5.1(b) $r = 500$ nm and for the case of hemispherical cavities depicted in Fig. 5.1(c) we have also $r = 500$ nm.

Table 5.1. Integral difference in the useful absorption compared to a bare TFSC granted by the LTSs (three new ones and one old one) and by the ARC.

Angle°	LTS, design a	LTS, design b	LTS, design c	LTS of spheres	ARC
0	+13.08	+5.6	+14.26	+14.92	+8.43
30	+242.28	+242.77	+257.29	+16.42	+36.3
60	+81.25	+92.92	+85.96	+70.12	-1.3
Average	+112.21	+113.76	+119.17	+34.92	+31.97

Now, let me discuss the physics of the effect. For all three structures I have analyzed the local field distributions varying the structural periods and frequencies. Spheres half-submerged into AZO and hemispherical protrusions of AZO shown in two left panels of Fig. 5.1 form the light

nanojet of the incident plane wave absolutely similarly to its formation by spheres located on the top interface, as it was in the previous chapter. The light-collimating structure shown in Fig. 5.1(c) has a peculiarity that deserves to be clarified.

In work [49] one has theoretically revealed the light-trapping properties of submicron indentations made in the anti-reflective layer located on top of a TFSC. These dents were shaped as truncated cones. Prior to [49] it had been already known that such the nanopatterning improved the wide-angle operation of flat ARCs [84] – the dents make the reflectance less sensitive to the incidence angle. In [49] authors performed extensive simulations varying the geometric parameters of the dents and for sufficiently large dents I have revealed the increase of the absorption in the substrate accompanied by the transmitted light collimation. The increase of the absorption was non-uniform over the visible range – there were several local maxima. However, even at the minima the absorption was not lower than in the absence of the dents. The collimated beams had characteristic width of the order of 300-400 nm. The collimation was kept in the PV layer of the a-Si TFSC and authors claimed the possibility to use the dents shaped as truncated cones for the enhancement of TFSCs.

However, my further numerical studies have shown that their initial assumption was wrong. The formation of the collimated beam in the case of a truncated conical dent is less efficient than that in the case of a hemispherical dent. And in both cases it is not the collective effect but the effect of the isolated cavity – it does not vanish with the increase of the structural period. The increase of the absorption is much stronger for the dents with nearly micron diameter (for hemispherical dens it means $2r = 800 - 1200$ nm) than for the dents with diameters 400-600 nm studied in [49]. So, the formation of the collimated beam results from the refraction of the cavity modes.

This effect is similar to that revealed in work [83] for hemispherical dents on the surface of a hyperbolic metamaterial. An incident plane wave produces a package of spherical spatial harmonics in the cavity whose size has the order of the wavelength in free space and strongly exceeds the effective wavelength in the material. When the eigenmodes of the cavity refract into the material the tangential component of the wave vector is preserved. This results in the formation of the light beam with a very broad angular spectrum. In the case of the normal incidence the cavity modes are excited symmetrically in the horizontal plane. In this case the

angular spectrum of the refracted beam is rather similar to that of the Gaussian one. However, this is not a solid (cylindrical) Gaussian beam, there is also a tubular beam around it.

Further operation of the dents is similar to that of any LTS. Due to the light concentration the absorption in these collimated wave beams is much higher than in the case of a plane wave simply refracted into the substrate. The key issue here is the quality of the hemispherical cavity. My hemispherical dents collimate the incident wave much better than the truncated conical notches of [49]. This effect is weakly frequency selective because the hemispherical cavity is multiresonant.

Understanding this physical mechanism allowed us to optimize the LTS depicted in Fig. 5.1. We have found that the structure of hemispherical voids is better than two other counterparts. The formation of the light nanojet in the structures of Fig. 5.1(a) and (b) is not much less efficient and grant basically the same gain in the PV absorption (that dramatically exceeds the gain granted by our previous LTS). However, the design of Fig. 5.1(c) is slightly more advantageous. And what is more important, my simulations have shown that its reflectance weakly grows versus the structural period. The minimal reflectance corresponds to the case when the period equals to $2r = 1$ μm. However, the reflectance from the structure with twice larger period still is lower than that from the bare TFSC (without dents). These simulations promised a weak sensitivity of the backscattering losses to the defective regions of the experimental sample. Recall that our goal is to develop an LTS without a strong increase of backscattering losses due to fabrication defects. From this point of view, the array of hemispherical dents seems to be very advantageous compared to its counterparts.

5.2 Experimental and further numerical studies

I have fabricated several samples of a-Si TFSC with the following design parameters (from the bottom to the top): the rear electrode of AZO of thickness 300 nm, the n-doped a-Si (10^{20} 1/cm^3) of thickness 100 nm, the intrinsic a-Si of thickness 400 nm, the p-doped a-Si (10^{18} 1/cm^3 of thickness 100 nm, and the front electrode of AZO. In these samples, this 600 nm thick layer of AZO was patterned by an array of densely packed hemispherical micron-sized dents of radius $r = 600$ nm. These dents were filled with silica. The presence of silica was dictated by the fabrication tech-

nique described below. The optimal value for r was re-designed taking into account this silica filling. In our initial simulations of this experimental structure we assumed that the silica insertions are hemispherical inside the cavities, and the optimal value $r = 600$ nm was found namely from this assumption. Only the silica filling (not the geometric parameters of the experimental TFSC) changes the value for the optimal r compared to $r = 500$ nm obtained above for the void hemispheres. The beam collimation is not sensitive to the thickness of layers located beneath of the LTS.

We experimentally compared the absorption in these samples with that measured for the samples of bare SC and for the samples enhanced by an ARC. Since a flat layer of AZO with thickness as substantial as 600 nm brings noticeable optical losses and is never used in practical TFSCs, it would be incorrect to compare our textured samples with flat ones keeping the same 600 nm for the front electrode. Our reference samples comprised the top layer of AZO with thickness 300 nm. Judging upon the literature this value is maximal practically usable thickness of the AZO front electrode. For this thickness of AZO a 80 nm thick ARC of silica (see in the previous chapter) is not optimal. Here, the ARC was a layer of SiN with thickness 100 nm. This ARC grants similarly low reflection losses as those in the previous chapter.

The measurements of the backscattering losses for the textured samples (those with our new LTS) have shown that the keenest issue of our previous design was resolved. Even in the defective regions with isolated notches and their clusters the backscattering does not noticeably exceed the reflectance of the bare AZO. In the scale of square centimeters the operation of the structure together with defective regions keeps wide-angle anti-reflective and wide-angle light-trapping. Of course, due to the presence of the defects the increase of the PV absorption becomes not as spectacular as in the third column of Table 4.2. However, the significant enhancement keeps for the whole area of the SC. For our previous LTS of silica spheres the enhancement was shown only if we illuminated the regular domains of our LTS by a mm-wide beam. In the experiment described below we illuminate the SC by the wave beam of cm diameter.

It is also important to stress that the anti-reflective and light-trapping functionalities were achieved with the textured top electrode. There is no need in a special ARC on top of it.

5.2.1 Fabrication method and the obtained structure

My fabrication technique is as follows. I use ALD and ion beam etching (IBE) in the small copy of an industrial machine from Meyer Burger Technology AG. The IBE technique deals with a rather wide ion beam and is therefore much cheaper and faster than the ion beam lithography (that is based on nanofocused ion beams). It can process any samples up to wafer size operating as a nano-blade cutting the surface at any angle up to the grazing cutaway with a uniform beam of Ar ions. Etching rate is 20–50 nm/min.

First, I prepare a monolayer of colloidal silica microspheres like I did the previous LTS. The only difference – now the spheres form a monolayer not on top of AZO as in the previous chapter but on top of the PV layer. The substrate to which the colloidal spheres glue up is p-doped a-Si. The diameters of the silica spheres used for our new LTS is 1.2 μm. Deviations from this optimal diameter were smaller than 100 nm. And, what was most important for my purposes, the deviations from the sphericity of silica particles from nanoComposix Ltd. were negligible.

Next, I deposit a layer of AZO using ALD. It is seen in the SEM image of Fig. 5.2 that the film of AZO was successfully deposited on the amorphous silicon substrate filling all the gaps between the spheres and forming a layer of needed thickness $h = r$. ALD was done with the ratio of steps 19:1 (19 steps of ZnO to 1 step of Al_2O_3 deposition). In Fig. 5.2 the top half of the structure is removed. This was done with the qulity offered by IBE. The removal results in a regular arrangement of the high-quality hemispherical cavities filled with the silica microparticles. The process of removal is very fast – takes 10.5 minutes for the area of 10 cm^2.

After IBE the top half of a silica sphere does not completely disappear. Unlike our expectations, we obtain the surface covered by protrusions shaped as nanocones. In other words, silica insertions in our hemispherical dents have the semi-diamond shape. The regular arrangement of these insertions in our hemispherical dents turned out to be useful for the reduction of backscattering losses. The reflectance drastically reduces. Color map of Fig. 5.1(c) corresponds to the reflectance nearly equal to 10%, that is close to the reflectance from bare ARC. The hemispherical inclusions of silica in the dents reduce the reflectance only slightly. From our preliminary simulations, in which silica insertions were hemispherical I expected the anti-reflective functionality of the textured AZO electrode

only for large incidence angles. However, the reality turned out to be better than we expected. The insertions are semi-diamond and their conical protrusions reduce the reflection losses operating like a transition layer on top of a flat surface.

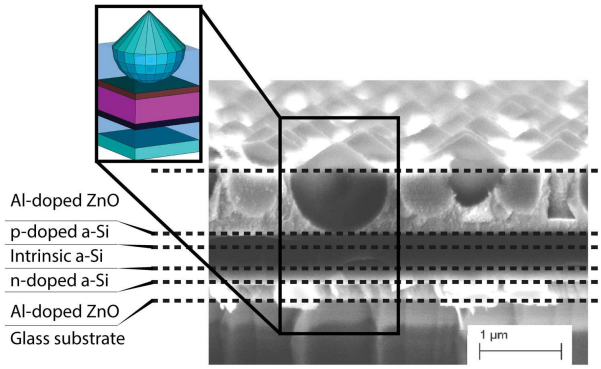

Figure 5.2. SEM image of the side cross section of the whole structure with the data on constitutive layers.

In this study I have intentionally made the structure transparent because my goal was to measure the absorbance in the PV layer due to light trapping. Here I followed to the logics of work [86]. The presence of the metal bottom electrode in a working TFSC will change this absorption quantitatively, but qualitatively the high gain should keep. This expectation was confirmed by numerical simulations using CST Studio. The gain in the PV absorption granted by such the patterning of AZO layer is maximal at λ =550-850 nm – this is the range where the hemispherical cavity operates as a microlens. The integral gain averaged over the incidence angles is equal 22%.

5.2.2 Post-fabrication simulations and discussion

The regularity of the dents and, respectively, the high quality of the hemispherical cavities responsible for the light trapping is granted by my fabrication technique. However, even in the defective regions isolated nanocones and their clusters scatter weakly and do not increase the reflectance as drastically as described in the previous chapter. I made extended numerical simulations of the periodic structure with period much larger than $2r$ and got a theoretical evidence of weak backscattering by the silica insertions even for large periods. Thus, insertions of silica improve the antireflective operation in the regular part of my LTS and do not increase the

backscattering compared to the bare surface in the defective areas.

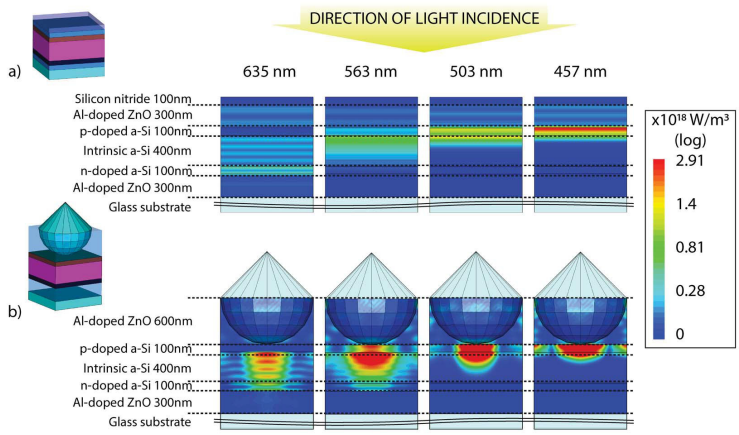

Figure 5.3. Comparison of the electromagnetic flux density in the reference (a) and suggested (b) structures at 4 wavelengths.

Finally, it remains to theoretically confirm simulations the claimed mechanism of light-trapping – the collimation of light by hemispherical dents in AZO, now taking into account the semi-diamond shape of silica insertions. It turned out that this shape did not affect the formation of the collimated beam. In Fig. 5.3 I present the results of corresponding simulations for four occasionally chosen wavelengths from the operation band of the SC. One can see the drastic difference in the spatial distributions of the electromagnetic flux density obtained for the suggested structure with LTS and in the reference structure with a flat anti-reflective coating. In the last case we observe the plane-wave transmission with its standard decay rate. In the case of LTS we see the collimated cylindrical wave beam composed under every dent. At λ =457 and λ =503 nm we also see the second collimated beam – tubular one – at the sides of the central one. At all wavelengths between 400 and 650 nm there is the field concentration preventing the parasitic transmittance.

5.2.3 Measurement results and conclusions

As it was already pointed out the samples with geometry shown in Fig. 5.2 were compared with their flat analogues – covered by an ARC and bare ones. Putting our samples in the integrating sphere and analyzing the scattering losses with the UV-Vis spectroscopic device Lambda 950 from Perkin Elmer Inc, I saw that even for the normal incidence (when the expected advantages of my LTS are minimal) the suggested structure does

not reflect more light than the structure with ARC. This confirmed robustness of the antireflection functionality to the fabrication defects.

Next, I indirectly measured the spectrum of the power absorbance found through the reflectance and transmittance directly measured for the range of incidence angles from 0 to 60°. In accordance to calculations, the integral absorbance corresponding to both layers of AZO electrodes does not exceed 3% and the absorbance of the n-doped layer of a-Si is nearly 1%. The total parasitic absorption does not exceed the deviations of the measured absorption for different samples.

Therefore, with acceptable accuracy, that corresponds to the deviations measured (shown in Fig. 5.4 for both experimental curves) we may attribute all the measured absorbance to the PV layer (intrinsic and p-doped sublayers).

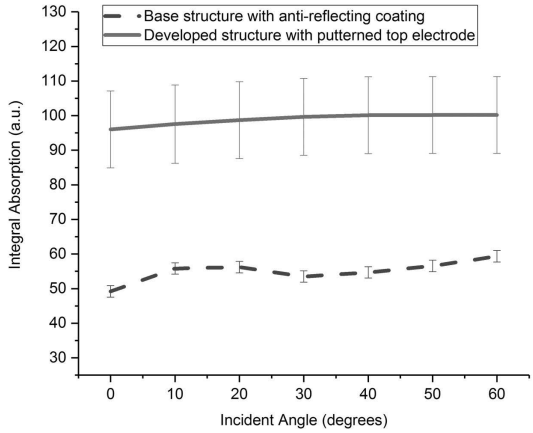

Figure 5.4. Integral power absorbance measured for the structure with the ARC on top of the front electrode and for the structure with the textured top electrode at different incident angles. Statistical deviations include both deviations for the different samples of the same type and the intrinsic measurement error.

I measured the power absorbance at different wavelengths of the operation band (400-700 nm) and incidence angles. In Fig. 5.4 we show the integral absorbance of our structure. Its almost 90% increase compared to the ARC is the main result of my study. The angular dependence of the gain is smooth and does not contain a maximum at $\theta = 30^\circ$ predicted by the theory for the regular structure. It is not surprising in presence of numerous defective areas in our 5 cm large samples. However, the advantage keeps for a large-area nanostructured LTS in spite of these defects with respect to the flat ARC having no defects. This result merits to finalize my studies.

Really, our LTS incorporated into the top electrode offers a significant reduction to both reflection and parasitic transmission. For TFSCs based on the a-Si with the non-polished rear electrode there is no one known counterpart that could equate our structure in the optical efficiency. Our structure with roughly the same bandwidth and angular dependency of reflection as a TFSC enhanced by a moth-eye ARC surpasses it in what concerns the gain in the PV absorption. It is really striking that such the result was obtained in spite of the presence of defects.

Offered structure can be fabricated in the affordable way that makes it attractive for industrial adaptation. An only expensive operation is the application of the ALD machine in order to prepare the transparent electrodes. However, ALD is developing fast and becoming cheaper and faster than earlier. In accordance with [37] ALD has good perspectives in the mass production of SCs.

So, I have introduced and fabricated a new LTS integrated with the top electrode that looks very promising for a-Si TFSCs. My LTS is affordable and efficient (broadband, almost lossless and grants the wide-angle operation). It is much more advantageous than the anti-reflective coating and its industrial adaptation may give a new pulse to solar photovoltaics based on amorphous silicon.

6. Summary of Publications

[I] Perfect plasmonic absorbers for photovoltaic applications

A novel regime of perfect absorption in a thin plasmonic layer corresponds to a collective mode of an array of plasmonic nanospheres. In our theoretical study we show that the absorption of the incident light occurs mainly in the semiconductor material hosting plasmonic nanospheres, whereas the absorption in the metal is very small. The regime survives when the uniform host layer is replaced by a practical photovoltaic cell. Trapping the light allows the thickness of the doped semiconductor to be reduced to values for which the degradation under light exposure should be insufficient. The light-trapping regime is compatible with both the metal-backed variant of the photovoltaic cell and its semitransparent variant when both electrodes are preformed of a conductive oxide. Negligible parasitic losses, a variety of design solutions and a reasonable operational band make our perfect plasmonic absorbers promising for photovoltaic applications.

[II] Enhancement of Perovskite Solar Cells by Plasmonic Nanoparticles

Synthetic perovskites with photovoltaic properties open a new era in solar photovoltaics. Due to high optical absorption perovskite-based thin-film solar cells are usually considered as fully absorbing solar radiation on condition of ideal blooming. However, it is not really so. The analysis of the literature data has shown that the absorbance of all photovoltaic perovskites has the spectral hole at infrared frequencies where the solar radiation spectrum has a small local peak. This absorption spectral dip results in the decrease of the optical efficiency of thin-film perovskite solar

cells and blocks the prospective of perovskite photodiodes to be used for sensing purposes in this range. In our work we show that to cure this shortage is possible complementing the basic structure by an inexpensive plasmonic array of nanospheres.

[III] A non-resonant dielectric metamaterial for the enhancement of thin-film solar cells

Recently, we have suggested a dielectric metamaterial composed of an array of submicron dielectric spheres located on top of an amorphous thin-film solar cell. We have theoretically shown that this metamaterial can decrease the reflection and simultaneously suppress the transmission through the photovoltaic layer because it transforms the incident plane wave into a set of focused light beams. This theoretical concept has been strongly developed and experimentally confirmed in the present paper. Here we consider the metamaterial for oblique angle illumination, redesign the solar cell and present a detailed experimental study of the whole structure. In contrast to our previous theoretical study we show that our omnidirectional light-trapping structure may operate better than the optimized flat coating obtained by plasmaenhanced chemical vapor deposition.

[IV] All Angle Light-Trapping Electrode for Photovoltaic Cells

In this paper we experimentally show that a submicron layer of a transparent conducting oxide that may serve a top electrode of a photovoltaic cell based on amorphous silicon when properly patterned by notches becomes an efficient light-trapping structure. This is so for a-Si thin-film solar cells with the best design parameters (p-i-n structure with optimal thickness of intrinsic and doped layers). The nanopatterned layer of transparent conducting oxide reduces both the light reflectance from the photovoltaic cell and transmittance through the photovoltaic layers for normal incidence and for all incidence angles. We explain the physical mechanism of our light-trapping effect, prove that namely this mechanism realized in our structure and show that the nanopatterning is achievable in a rather easy and affordable way that makes our method of the solar cell enhancement attractive for industrial adaptation.

7. Conclusions

This thesis reports my doctoral studies in the field of light-trapping structure for planar multilayer thin-film photovoltaic diodes. In this report we consequently pass from plasmonic light-trapping structures enhancing the PV absorption of photodiodes in a narrow band to broadband all-dielectric light-trapping structures which were fabricated and successfully tested experimentally.

In the theoretical part of the thesis our narrowband photodiodes operate as electric generators illuminated by artificial light. We found a suitable biomedical application. Also, they can be perovskite solar cells – then our plasmonic light-trapping structure compensates their narrowband spectral dip in the absorption.

Restricting our plasmonic LTSs by the easy requirement of narrowband operation we obtain a possibility to combine the advantageous regime of light trapping with the simplicity of the array. The particles are nanospheres or nanoshells available in colloids. The novelty of this study is the use of the collective plasmon resonance of an array of densely arranged nanospheres. In this regime the plasmonic hot spots do not intersect with the metal elements and the parasitic dissipation in them is avoided. This type of the resonance has never been previously utilized for light-trapping.

In the experimental part of the thesis I have suggested and studied two new types of broadband affordable light-trapping structures with wide-angle operation. The first one was a monolayer of densely-packed micron-sized spheres of silica. This monolayer operates as a solid antireflective coating for the reflected light and as an array of microlenses for the light transmitted into substrate. The light concentration increases the local absorption and the LTS offers a broadband light-trapping operation. This operation is especially advantageous for large incidence angles due to a new regime of focusing the light that we called the cascade light collima-

tion. The contest with an optimal anti-reflecting coating was gained by offerd LTS inspecting the solar cell efficiency in the wide angular spectrum. I have developed a very simple and affordable technique for manufacturing such LTSs on top of a-Si solar cells. The measurements have confirmed my numerical simulations with high accuracy.

This structure had a drawback – it was not robust to the harmful action of its defective areas. In these defects the LTS was either absent or substituted by isolated spheres and their small clusters. These areas have mm sizes (as well as high-quality areas) and are very harmful for the operation of large-area samples. Therefore, in our experiments we used the collimated light beam and illuminate only the properly prepared areas of the experimental LTS. I saw that we need to design an alternative LTS which would be less sensitive to fabrication defects.

With this purpose I have revealed a new mechanism of light collimation rather similar to the formation of a submicron-collimated beam (nanojet) by a micron-sized dielectric sphere. Namely, hemispherical micron-sized dents also create a nanojet in a transparent medium. An array of densely packed hemispherical dents prepared on top of the front electrode operates as an LTS that is much more efficient than the previous one. Moreover, the anti-reflective operation of this new LTS is affected by the defects not so strongly as my previous LTS.

I have checked experimentally these theoretical expectations. Using the self-assembly, atomic layer deposition and ion-beam etching I fabricated this structure and the reality turned out to be even better than I had expected. My structures comprised a set of silica nancones on top of it and these nanocones decreased the reflection similarly to the anti-reflective effect of the so-called black silicon. This unexpected shape of the silica insertions located in the hemispherical dents did not decrease the light-trapping effect and its action was fully positive. Therefore, in practice the useful absorption grows due to the presence of my LTS almost twice compared to the same structure enhanced by the ARC (and more than 2.5 times compared to the bare structure). This increase holds for 5 cm large samples in spite of numerous defective regions on the surface.

These experimental results finalize my efforts and this dissertation. I believe in the high importance of my work that may open a new door for the further development of the amorphous silicon photovoltaics.

References

[1] A.L. Fahrenbruch and H. Bube. Fundamentals of Solar Cells: Photovoltaic Solar Energy Conversion, (1983) New York: Academic Press, USA

[2] F.G. Knoll. Radiation detection and measurement (2010) 4th Ed. Wiley, Hoboken, NJ, USA.

[3] J.F. Cox. Fundamentals of Linear Electronics: Integrated and Discrete (2001) 2d Ed. Delmar/Thomson Learning, Inc., Alnay, NY, USA.

[4] F. Tavernier, and M. Steyaert. High-Speed Optical Receivers with Integrated Photodiode in Nanoscale CMOS (2011) Springer, NY, USA.

[5] A. Marti and A. Luque, Next-generation photovoltaics (2004) Institute of Physics Publishing, Bristole, UK - Philadelphia, USA

[6] J. Nelson, The Physics of Solar Cells (2003) Imperial College Press, London, UK.

[7] Ultra-Low-Cost Solar Electricity Cells, An Overview of Nanosolar's Cell Technology Platform, Nanosolar, Inc. White Paper (2009), available at www.catharinafonds.nl/wp-content/uploads/2010/03/NanosolarCellWhitePaper.pdf

[8] Milichko, V.A., Shalin, A.S., Mukhin, I.S., Kovrov, A.E., Krasilin, A.A., Vinogradov, A.V., Belov, P.A. and Simovski, C.R., (2016) Solar photovoltaics: current state and trends. *Physics Uspekhi*, 59(8), p.727.

[9] Solar Energy Industries Association, *U.S. Solar Market Insight Report* (2011) Year-in-Review.

[10] A. S. Shalin (2011) *Quantum Electronics* , 41, 163

[11] *Thin-Film Solar Cells: Next Generation Photovoltaics and Its Applications*, Y. Hamakawa, Ed. (2004) Berlin: Springer, Germany

[12] Wang, P.H., M. Theuring, M. Vehse, V. Steenhoff, C. Agert, A.G. and Brolo. Light trapping in a-Si:H thin film solar cells using silver nanostructures, *AIP Advances* 7(1), (2017): 015019.

[13] Tamang, A., H. Sai, V. Jovanov, M.I. Hossain, K. Matsubara, and D. Knipp. On the interplay of cell thickness and optimum period of silicon thin-film solar cells: light trapping and plasmonic losses, (2016) *Prog. Photovolt: Res. Appl.* 24, 379–388.

[14] Ha, K., E. Jang, S. Jang, J.-K. Lee, M.S. Jang, H. Choi, J.-S. Cho, and M. Choet. A light-trapping strategy for nanocrystalline silicon thin-film solar cells using three-dimensionally assembled nanoparticle structures, (2016) *Nanotechnology* 27(5), 055403.

[15] T. Matsui et al., in: *Abstracts of 28th European Photovoltaic Solar Energy Conf. and Exhibition*, 30 September – 4 October 2013, Paris, France, p. 2213

[16] Golschmidt, V. M. Die Gesetze der Krystallochemie. *Die Naturwissenschaften* (1926). 21 (21): 477–485.

[17] F. Di Giacomo, A. Fakharuddin, R. Josec and T.M. Brown, Progress, challenges and perspectives in flexible perovskite solar cells *Energy Environ. Sci.* 9, 3007-3035 (2016)

[18] D. Langley, G. Giusti, C. Mayousse, C. Celle, D. Bellet and J.-P. Simonato, Flexible transparent conductive materials based on silver nanowire networks: a review, *Nanotechnology* 24, 0957 (2013)

[19] M. Luo, Y. Liu, W. Huang, W. Qiao, Y. Zhou, Y. Ye, and L.-S. Chen, Towards flexible transparent electrodes based on carbon and metallic materials, *Micromachines* 8, 12 (2017)

[20] Bermel, P., Luo, C., Zeng, L., Kimerling, L. C., Joannopoulos, J. D. (2007). Improving thin-film crystalline silicon solar cell efficiencies with photonic crystals. Optics express, 15(25), 16986-17000.

[21] S. B. Mallick, M. Agrawal, and P. Peumans, Opt. Express (2007). 18, 5691

[22] V. E. Ferry, L. A. Sweatlock, D. Pacifici, and H. A. Atwater, Nano Lett. (2008), 8, 4391

[23] K. R. Catchpole and A. Polman, Appl. Phys. Lett. (2008), 93 191113

[24] C. Rockstuhl and F. Lederer, Appl. Phys. lett. (2009), 94, 213102

[25] H. A. Atwater and A. Polman, Nature Mat. (2010), 9, 205

[26] D. M. Callahan, J. N. Munday, and H. A. Atwater, Nano Lett. (2012), 12, 214

[27] Y. Wang, T. Sun, T. Paudel, Y. Zhang, Zh. Ren, and K. Kempa, Nano Lett. (2012), 12, 440

[28] P. A. Spinelli, V. E. Ferry, J van de Groep, M. van Lare, M. A. Verschuuren, R. E. I. Schropp, H. A. Atwater, and A. Polman, J. Optics (2012), 14, 024002

[29] Simovski, Constantin, et al. Enhanced efficiency of light-trapping nanoantenna arrays for thin-film solar cells. Optics express 21.104 (2013): A714-A725.

[30] Voroshilov, Pavel M., and Constantin R. Simovski. Leaky dominomodes in regular arrays of substantially thick metal nanostrips. *Photonics and Nanostructures-Fundamentals and Applications* 20 (2016): 18-30.

[31] J. Grandidier, D. M. Callahan, J. N. Munday, and H. A. Atwater, Adv. Mater. (2011), 23, 1272

[32] Spinelli, P., M. A. Verschuuren, and A. Polman. "Broadband omnidirectional antireflection coating based on subwavelength surface Mie resonators." Nature communications 3 (2012): 692.

[33] Stutenbaumer, U., Mesfin, B. and Beneberu, S., (1999). Determination of the optical constants and dielectric functions of thin film a-Si:H solar cell layers, *Solar energy materials and solar cells*, 57(1), pp.49-59.

[34] Wang, Y., Chen, L., Yang, H., Guo, Q., Zhou, W. and Tao, M., (2010). Large-area self assembled monolayers of silica microspheres formed by dip coating. *Texas Univ at Arlington Dept of ElectricalEngineering*.

[35] Lee, D.J., Kim, H.M., Kwon, J.Y., Choi, H., Kim, S.H. and Kim, K.B., (2011). Structural and Electrical Properties of Atomic Layer Deposited Al-doped ZnO Films. *Advanced Functional Materials*, 21(3), pp.448-455.

[36] I. S. Sinev, P. M. Voroshilov, I. S. Mukhin, A. I. Denisyuk, M. E. Guzhva, A. K. Samusev, P. A. Belov, and C. R. Simovski, (2015) Demonstration of unusual nanoantenna array modes through direct reconstruction of the near-field signal, *Nanoscale* 7, 765.

[37] Lubitz, Michael, Phillip A. Medina IV, Aleks Antic, Joseph T. Rosin, and Bradley D. Fahlman. Cost-Effective Systems for Atomic Layer Deposition. *Journal of Chemical Education* 91, no. 7 (2014): 1022-1027.

[38] Y. Ra'di, V.S. Asadchy, S.U. Kosulnikov, M.M. Omelyanovich, D. Morits, A.V. Osipov, C.R. Simovski, and S.A. Tretyakov, (2015) Full Light Absorption in Single Arrays of Spherical Nanoparticles, *ACS Photonics*, 2, 653

[39] P. B. Johnson and R. W. Christy, (1972) Optical Constants of the Noble Metals *Phys. Rev. B* 6, 4370

[40] D.-H. Kim, R. Ghaffari, N. Lu, and J. A. Rogers, (2012) Flexible and Stretchable Electronics for Biointegrated Devices, *Annual Reviews of Biomedical Engineering* 14, 113

[41] P. Mandal, (2016) Plasmonic perfect absorber for refractive index sensing and SERS, *Plasmonics* 11(1), 223-229

[42] Y. Ra'di, C. Simovski and S. Tretyakov, (2015) Thin Perfect Absorbers for Electromagnetic Waves: Theory, Design, and Realizations *Phys. Rev. Applied* 3, 037001

[43] Y. Ra'di, V.S. Asadchy, and S.A. Tretyakov, Total absorption of electromagnetic waves in ultimately thin layers, (2013) *IEEE Trans. Antennas Propag*, 61, 4606-4614

[44] M. Albooyeh and C.R. Simovski, Huge local field enhancement in perfect plasmonic absorbers, (2012) *Opt. Express* 20, 21888-21895

[45] M. Decker, I. Staude, M. Falkner, J. Dominguez, D. N. Neshev, I. Brener, T. Pertsch , and Y. S. Kivshar, (2015) High-Efficiency Dielectric Huygens' Surfaces, *Adv. Opt. Mat.* 3(6), 813–820

[46] A. V. Kildishev, A. Boltasseva, and V. M. Shalaev, (2013) *Planar Photonics with Metasurfaces*, Science 339, 1232009

[47] Y. Yu, V. E. Ferry, A. P. Alivisatos, and L. Cao,(2012) *Nano Lett.*, 12, 3674

[48] J. Grandidier, R. A. Weitekamp, M. G. Deceglie, D. M. Callahan, C. Battaglia, C. R. Bukowsky, C. Ballif, R. H. Grubbs, and H. A. Atwater, (2012) *Physica Status Solidi A* 206(2), 193-194

[49] Voroshilov, P. M., Simovski, C. R., Belov, P. A. and Shalin, A. S., (2015). Light-trapping and antireflective coatings for amorphous Si-based thin film solar cells. *Journal of Applied Physics*, 117(20), p.203101

[50] Sinev, Ivan S., et al. (2015) Demonstration of unusual nanoantenna array modes through direct reconstruction of the near-field signal. *Nanoscale* 7.2, 765-770.

[51] Dmitriev, P. A., et al. (2016) Laser fabrication of crystalline silicon nanoresonators from an amorphous film for low-loss all-dielectric nanophotonics. *Nanoscale* 8.9, 5043-5048.

[52] A. Ecija, K. Vidal, A. Larranaga, L. Ortega-San-Martin, and M.I. Arriortua, Synthetic Methods for Perovskite Materials — Structure and Morphology, in: Advances in Crystallization Processes, Y. Mastai, Ed., InTech Publisher, Rieka–Shanghai, 486–506 (2012)

[53] A. Kojima, K. Teshima, Y. Shirai, T. Miyasaka, Organo-metal halide perovskites as visible-light sensitizers for photovoltaic cells. J. Am. Chem. Soc. 131, 6050—6051 (2009)

[54] H.S. Jung and N.-G. Park, Perovskite solar cells: From materials to devices, Small 11, 10–25 (2015)

[55] B. Wang, X. Xiao, T. Chen, Perovskite photovoltaics: a high-efficiency newcomer to the solar cell family, Nanoscale 6, 12287–12297 (2014)

[56] Q, Shen, Y. Ogomi, J. Chang, T. Toyoda, K. Fujiwara, K. Yoshino, K. Sato, K. Yamazaki, M. Akimoto, Y. Kuga, K. Katayamad, and S. Hayase, Optical absorption, charge separation and recombination dynamics in Sn/Pb cocktail perovskite solar cells and their relationships to photovoltaic performances, European Journal of Chemical Physics and Physical Chemistry 15, 1062–1069 (2014)

[57] M.-E. Ragoussia and T. Torres, New generation solar cells: concepts, trends, Chem. Commun. 51, 3957–3972 (2015)

[58] Qi Chena, Nicholas De Marcoa, Yang (Michael) Yanga, Tze-Bin Songa, Chun-Chao Chena, Hongxiang Zhaoa, Ziruo Honga, Huan-

ping Zhoua, Yang Yanga, The organic-inorganic hybrid halide perovskite for optoelectronic applications, Nano Today 10, 355–396 (2015)

[59] Mohd S. Alias, Yang Yang, Tien K. Ng, Ibrahim Dursun, Dong Shi, Makhsud I. Saidaminov, Davide Priante, Osman M. Bakr, and Boon S. Ooi, Enhanced Etching, Surface Damage Recovery, and Submicron Patterning of Hybrid Perovskites using a Chemically Gas-Assisted Focused-Ion Beam for Subwavelength Grating Photonic Applications, J. Phys. Chem. Lett., 7, 137–142 (2016)

[60] J. Tommila, A. Aho, A. Tukiainen, Moth-eye antireflection coating fabricated by nanoimprint lithography on 1 eV dilute nitride solar cell, Prog. Photov. Res. Appl. 21 1158–1162 (2012)

[61] H.J. Snaith, Perovskites: the emergence of a new era for low-cost, high-efficiency solar cells, J. Phys. Chem. Lett. 4, 3623–3630 (2013)

[62] S.B. Mallick, M. Agrawal, and P. Peumans, Optimal light trapping in ultra-thin photonic crystal crystalline silicon solar cells, Opt. Express 18: 5691 (2007)

[63] J.M. Ball, S.D. Stranks, M.T. Hörantner, S. Hüttner, W. Zhang, E.J.W. Crossland, I. Ramirez, M. Riede, M.B. Johnston, R.H. Friend and H.J. Snaith, Optical properties and limiting photocurrent of thin-film perovskite solar cells, Energy Environ. Sci., 8, 602 (2015)

[64] P.P. Boix, K. Nonomura, N. Mathews, and S.G. Mhaisalkar, Current progress and future perspectives for organic/inorganic perovskite solar cells, Materials Today 17(1) 16-23 (2014)

[65] T. Baikie, Y. Fang, J.M. Kadro; M. Schreyer, F. Wei, S.G. Mhaisalkar, M. Graetzel, and T.J. White, Synthesis and crystal chemistry of the hybrid perovskite (CH3NH3) PbI3 for solid-state sensitised solar cell applications, J. Mater. Chemistry A 1(18), p. 5628-5641, 2013

[66] M. Omelyanovich, Y. Ra'di and C. Simovski, Perfect plasmonic absorbers for photovoltaic applications, Journal of Optics, 17, 125901 (2015)

[67] D. A. Willis and V. Grosu, Microdroplet deposition by laser-induced forward transfer, Appl. Phys. Lett. 86, 244103 (2005).

[68] A.I. Kuznetsov, A.B. Evlyukhin, M.R. Goncalves, C. Reinhardt, A. Koroleva, M.L. Arnedillo, R. Kiyan, O. Marti, and B.N. Chichkov, Laser fabrication of large-scale nanoparticle arrays for sensing applications, ACS Nano 5, 4843 (2011)

[69] U. Zywietz, A. B. Evlyukhin, C. Reinhardt, and B. N. Chichkov, Laser printing of silicon nanoparticles with resonant optical electric and magnetic responses, Nature Comm. 5, 3402 (2014)

[70] P. Dmitriev, S.V. Makarov, V. Milichko, I. Mukhin, A. Gudovskikh, A. Sitnikova, A. Samusev, A. Krasnok, and P. Belov, Laser fabrication of crystalline silicon nanoresonators from an amorphous film for low-loss all-dielectric nanophotonics, Nanoscale (2015)

[71] P. Bermel, C. Luo, L. Zeng, L. C. Kimerling, and J. D. Joannopoulos, Opt. Express 15, 16986 (2007)

[72] S. Pillai, K. R. Catchpole, T. Trupke, and M. A. Green, J. Appl. Phys. 101, 093105 (2007)

[73] H. A. Atwater and A. Polman, Nature Mater. 9, 205 (2010)

[74] D. M. Callahan, J. N. Munday, and H. A. Atwater, Nano Lett. 12, 214 (2012)

[75] Z. Yu, A. Raman, and S. Fan, Opt. Express 18, A366 (2010)

[76] E. Hecht, (1987) *Optics* (2nd ed.) Addison Wesley, NY, USA.

[77] Z. Chen, A. Taflove, and V. Backman, *Opt. Express* 12, 1214 (2004)

[78] A. V. Itagi and W. A. Challener, *J. Opt. Soc. Am. A* 22, 2847 (2005)

[79] C. Clavero, Plasmon-induced hot-electron generation at nanoparticle/metaloxide interfaces for photovoltaic and photocatalytic devices, Nat. Photonics 8, 95—103 (2014)

[80] H. Chalabi and M. L. Brongersma, Plasmonics: harvest season for hot electrons, Nat. Nanotechnol. 8, 229—231 (2013)

[81] F. Pastorelli, S. Bidault, J. Martorell, N. Bonod, Self-assembled plasmonic oligomers for organic photovoltaics, Adv. Opt. Mat. 2, 171–175 (2014)

[82] Omelyanovich, M., Ovchinnikov, V. and Simovski, C., A non-resonant dielectric metamaterial for the enhancement of thin-film solar cells. *Journal of Optics*, 17(2), p.025102. (2015)

[83] Valagiannopoulos, C.A., Mirmoosa, M.S., Nefedov, I.S., Tretyakov, S.A. and Simovski, C.R., Hyperbolic-metamaterial antennas for broadband enhancement of dipole emission to free space. *Journal of Applied Physics*, 116(16), p.163106, (2014)

[84] J.Y. Chen and K.W. Sun, *Solar Energy Mater. Solar Cells* 94, 629 (2010).

[85] Dhakal, Tara, et al. "Transmittance from visible to mid infra-red in AZO films grown by atomic layer deposition system." Solar Energy 86.5 (2012): 1306-1312.

[86] Stutenbaumer, Ulrich, Belayneh Mesfin, and Solomon Beneberu. "Determination of the optical constants and dielectric functions of thin film a-Si: H solar cell layers." Solar energy materials and solar cells 57, no. 1 (1999): 49-59.

[87] V. G. Veselago, The electrodynamics of substances with simultaneously negative values of ε and μ, Sov. Phys. Usp. 10, 509 (1968).

[88] D. R. Smith, W. J. Padilla, D. C. Vier, S. C. Nemat-Nasser and S. Schultz, Composite medium with simultaneously negative permeability and permittivity, Phys. Rev. Lett. 84, 4184 (2000).

[89] D. R. Smith and D. Schurig, Electromagnetic wave propagation in media with indefinite permittivity and permeability tensors, Phys. Rev. Lett. 90, 077405 (2003).

[90] Z. Liu, H. Lee, Y. Xiong, C. Sun and X. Zhang, Far-field optical hyperlens magnifying sub-diffraction-limited objects, Science 315, 1686 (2007).

[91] K. Domanski, J. Correa-Baena, N. Mine, M. Nazeeruddin, A. Abate, M. Saliba, W. Tress, A. Hagfeldt, and M. Grätzel ACS Nano 10 (6), 6306-6314 (2016)

Aalto-DD 37/2018

ISBN 978-952-60-7869-4 (printed)
ISBN 978-952-60-7870-0 (pdf)
ISSN-L 1799-4934
ISSN 1799-4934 (printed)
ISSN 1799-4942 (pdf)

Aalto University
School of Electrical Engineering
Department of Electronics and Nanoengineering
www.aalto.fi

BUSINESS +
ECONOMY

ART +
DESIGN +
ARCHITECTURE

SCIENCE +
TECHNOLOGY

CROSSOVER

DOCTORAL
DISSERTATIONS